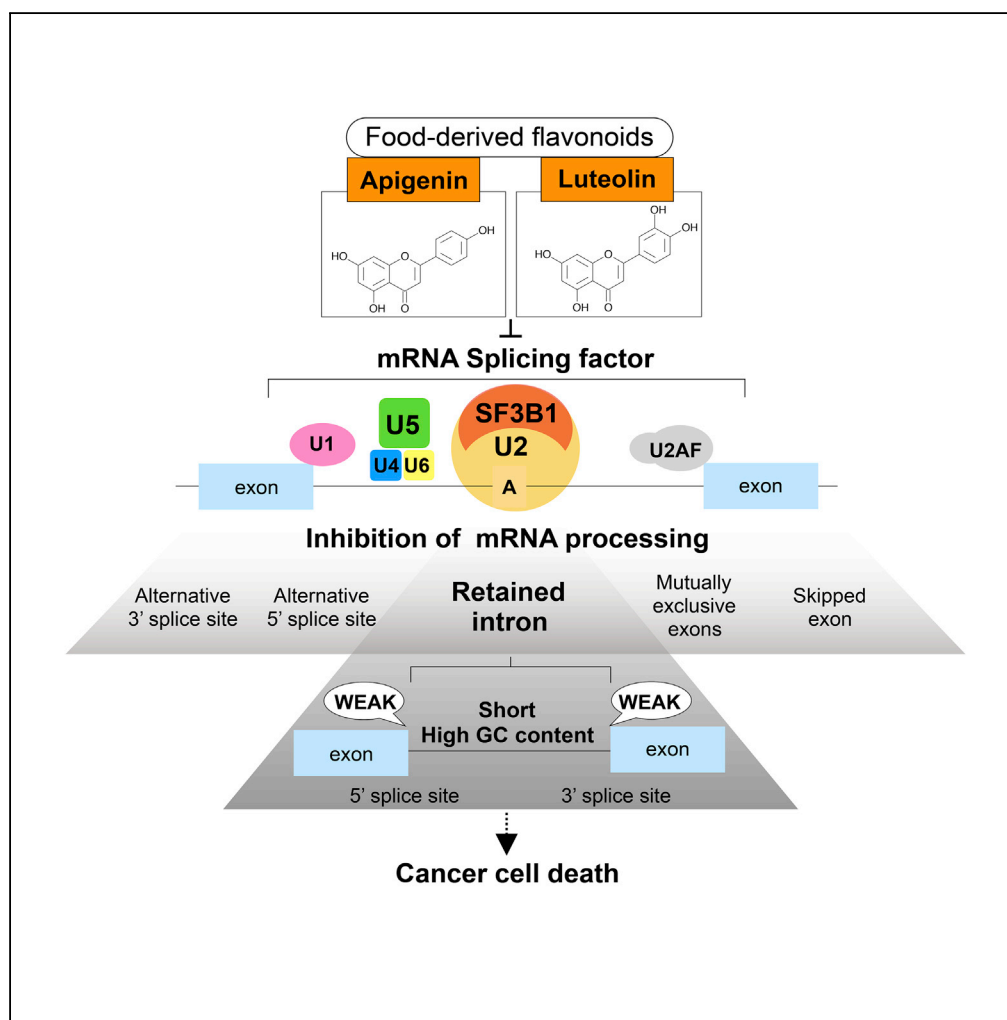Article

Food-Derived Compounds Apigenin and Luteolin Modulate mRNA Splicing of Introns with Weak Splice Sites

Masashi Kurata,
Naoko Fujiwara,
Ken-ichi Fujita, ...,
Nobuyuki
Takahashi,
Yasuyuki Shibuya,
Seiji Masuda

masuda@kais.kyoto-u.ac.jp

HIGHLIGHTS
Food-derived
compounds, apigenin and
luteolin, modulate mRNA
splicing

The treatment of these
flavonoids causes
numerous alternative
splicing events

Splicing of introns with
weak splice sites tend to
be inhibited by these
flavonoids

Tumorigenic cells are
more sensitive to these
flavonoids than non-
tumorigenic cells

Article

Food-Derived Compounds Apigenin and Luteolin Modulate mRNA Splicing of Introns with Weak Splice Sites

Masashi Kurata,[1,2] Naoko Fujiwara,[1] Ken-ichi Fujita,[1] Yasutaka Yamanaka,[1] Shigeto Seno,[3] Hisato Kobayashi,[4,7] Yusaku Miyamae,[5] Nobuyuki Takahashi,[6] Yasuyuki Shibuya,[2] and Seiji Masuda[1,8,*]

SUMMARY

Cancer cells often exhibit extreme sensitivity to splicing inhibitors. We identified food-derived flavonoids, apigenin and luteolin, as compounds that modulate mRNA splicing at the genome-wide level, followed by proliferation inhibition. They bind to mRNA splicing-related proteins to induce a widespread change of splicing patterns in treated cells. Their inhibitory activity on splicing is relatively moderate, and introns with weak splice sites tend to be sensitive to them. Such introns remain unspliced, and the resulting intron-containing mRNAs are retained in the nucleus, resulting in the nuclear accumulation of poly(A)$^+$ RNAs in these flavonoid-treated cells. Tumorigenic cells are more susceptible to these flavonoids than nontumorigenic cells, both for the nuclear poly(A)$^+$ RNA-accumulating phenotype and cell viability. This study illustrates the possible mechanism of these flavonoids to suppress tumor progression *in vivo* that were demonstrated by previous studies and provides the potential of daily intake of moderate splicing inhibitors to prevent cancer development.

INTRODUCTION

Messenger RNA processing (5′ capping, splicing, and 3′ end processing) is a fundamental step in eukaryotic gene expression to sustain various cell functions, such as proliferation, survival, and differentiation (Maniatis and Reed, 2002; Millevoi and Vagner, 2009; Orphanides and Reinberg, 2002). Among them, mRNA splicing is a crucial process through which noncoding introns are removed from pre-mRNA by the spliceosome, composed of five snRNPs (small nuclear ribonucleoproteins: U1, U2, U4, U5, and U6 snRNPs) and an assembly of accessory proteins (Hoskins and Moore, 2012; Wahl and Lührmann, 2015). This machinery recognizes short consensus sequences in the pre-mRNA, at the 5′ splice site, the branchpoint sequence (BPS), and the 3′ splice site. Alternative splicing plays an important role in conferring remarkable variety on the eukaryotic transcriptome through the differential usage of splice sites (Kim et al., 2014; Pan et al., 2008; Wang et al., 2008). It has been suggested that abnormalities in mRNA splicing lead to many pathological conditions, such as cancer onset and progression (Scotti and Swanson, 2016; Yoshida et al., 2011). For this reason, the inhibition of inadequate splicing is attracting attention as an important therapeutic strategy (Daguenet et al., 2015; Hahn et al., 2015; Maguire et al., 2015; Nlend Nlend et al., 2010; Salton and Misteli, 2016).

Various studies to detect compounds with inhibitory activity on splicing have been performed, and these successfully identified several microorganism-derived compounds with activities that modulate mRNA splicing (Effenberger et al., 2017). For example, spliceostatin A, pladienolide B, GEX1A, and H3B-8800 inhibit pre-mRNA splicing by disturbing spliceosome complex formation via binding to a component of the SF3B complex, one of the constituents of U2 snRNP (Hasegawa et al., 2011; Kaida et al., 2007; Kotake et al., 2007; Seiler et al., 2018).

Regarding food-derived compounds, epigallocatechin gallate, apigenin, and resveratrol were first identified by their inhibitory effects on the growth of cancer cells and later revealed to induce the alternative splicing of several mRNAs (Arango et al., 2013; Markus et al., 2011; Sakla and Lorson, 2008). However, only a few reports to date have been published on food-derived compounds with the ability to modulate mRNA processing. Because various previous studies have focused on compounds with strong inhibitory effects on splicing, the compounds with relatively moderate activity, such as food-derived compounds, have been overlooked.

[1]Division of Integrated Life Sciences, Graduate School of Biostudies, Kyoto University, Kyoto 606-8502, Japan

[2]Department of Oral and Maxillofacial Surgery, Graduate School of Medical Sciences, Nagoya City University, Nagoya 467-8601, Japan

[3]Department of Bioinformatic Engineering, Graduate School of Information Science and Technology, Osaka University, Osaka 565-0871, Japan

[4]NODAI Genome Research Center, Tokyo University of Agriculture, Tokyo 156-8502, Japan

[5]Faculty of Life and Environmental Sciences, University of Tsukuba, Ibaraki 305-8572, Japan

[6]Department of Nutritional Science and Food Safety, Tokyo University of Agriculture, Tokyo 156-8502, Japan

[7]Present address: Department of Embryology, Nara Medical University, Nara 634-8521, Japan

[8]Lead Contact

*Correspondence: masuda@kais.kyoto-u.ac.jp

https://doi.org/10.1016/j.isci.2019.11.033

In our established method, a relatively moderate inhibitory effect on mRNA processing can be captured as bulk poly(A)$^+$ RNA accumulation in the nucleus (Fujita et al., 2012; Fujiwara et al., 2010). Utilizing our method, we previously screened food-derived compounds and identified mRNA processing inhibition activities in the soybean-derived isoflavonoid fraction and performed further analysis that elucidated that this activity was mainly exerted by compounds with a flavone skeleton (Kurata et al., 2016, 2017).

In this study, we assessed the activity of 21 compounds with a flavone skeleton to inhibit mRNA processing and found that two of these flavonoids with highly related structures, namely, apigenin and luteolin, exhibited the strongest activity. LC-MS/MS analysis of proteins bound to these compounds suggested that their cellular targets are mRNA splicing-related proteins. RNA-seq data revealed that many alternative splicing events were induced upon treatment with these flavonoids, strongly suggesting the effect of these compounds on mRNA splicing. Further extensive analysis of the sequence features of target introns indicated that these flavonoids tend to influence the splicing of introns with weak splice sites.

This study provides an effective approach to identify compounds exerting moderate inhibitory activity against mRNA processing, with a particular emphasis on the usefulness of global analysis to clarify the mechanisms underlying the perturbations induced by these compounds in mRNA processing. Using the method described in this study, previously overlooked chemical libraries, such as those of food-derived compounds, are worth revisiting as potential sources of compounds with moderate activity of modulating mRNA processing.

RESULTS

Apigenin and Luteolin Exhibit Inhibitory Activity against mRNA Processing

Previously, we identified several flavonoids that have inhibitory activity against mRNA processing (Kurata et al., 2016, 2017). In this study, we explored the structure-activity relationship of compounds with a flavone skeleton by RNA-FISH (Figures 1 and S1). GEX1A, a well-known splicing inhibitor, was used as a positive control. The structure of flavones contains a skeleton of diphenylpropane, namely, two benzene rings (A-ring and B-ring) linked via a closed pyran ring (C-ring) with a benzenic A-ring. In addition, they have a double bond between the 2 and 3 positions and a ketone at the 4 position of the C-ring. Among the 21 compounds tested, apigenin and luteolin exhibited the most intense and dose-dependent phenotype of accumulating poly(A)$^+$ RNA in the nucleus (Figures 2A–2C). These compounds harbor OH groups at the 5 and 7 positions of the A-ring, an OH group at the 4′ position of the B-ring, and a double bond in the C-ring as common structures, whereas an OH group at the 6 position of the A-ring, or the 2′ or 5′ position of the B-ring, appears to eliminate the flavonoids' activity on mRNA processing (Figures 1 and S1B). In apigenin- and luteolin-treated cells, poly(A)$^+$ RNAs mainly co-localized with SC35, a nuclear speckle marker protein, indicating the accumulation of RNAs residing within the nuclear speckles (Figure 2D). This phenomenon was also observed in cells treated with GEX1A.

mRNA Splicing Is a Candidate for the Cellular Target of Apigenin and Luteolin

The observed nuclear poly(A)$^+$ RNA accumulation in apigenin- and luteolin-treated cells may reflect the disruption of an mRNA export pathway (Lee et al., 2008). To examine this possibility, we assessed the subcellular localization of transiently expressed *β-globin* mRNA in control cells and apigenin- or luteolin-treated cells. Expressed reporter *β-globin* mRNA was visualized using Alexa Fluor 546-labeled *β-globin* FISH probe (Figures 3A and 3B). Even in cells exhibiting a prominent phenotype of poly(A)$^+$ RNA accumulation in the nucleus induced by treatment with these flavonoids, *β-globin* mRNA was exported to the cytoplasm as efficiently as in control cells, indicating that the general mRNA export machinery is not disturbed in these cells. In addition, the *β-globin* gene used in this assay contains introns with constitutive splice sites, suggesting that this reporter mRNA properly undergoes splicing. Indeed, when we assessed the splicing of this reporter mRNA, no obvious inhibition caused by these flavonoids was observed (Figure 3C). On the other hand, it has been reported that apigenin and luteolin treatment alters the splicing pattern of *Caspase-9* and *c-FLIP* into an apoptosis-inducible form, thus inhibiting the proliferation of cancer cells (Arango et al., 2013). Those previously described changes in splicing pattern, namely, the decreases in both *Caspase-9b*, a variant with skipping of exons 3–6, and *c-FLIP$_s$*, a variant with exon 7 instead of 8, were also induced by apigenin and luteolin treatment in our experimental conditions, implying that these flavonoids have some effect on splicing (Figure 3D). Supporting the idea that apigenin and luteolin affect splicing rather than export, the apigenin- and luteolin-derived nuclear speckle-associated poly(A)$^+$ RNA accumulation pattern was similar to that observed in cells depleted of SF3B1, a component of U2 snRNP

Name	Chemical formulas	A-ring				B-ring					C-ring		Inhibition of mRNA processing
		5	6	7	8	2'	3'	4'	5'	6'	3	Double bond	
Flavone												1	+
5-hydroxyflavone		-OH										1	−
7-hydroxyflavone				-OH								1	+
Chrysin		-OH		-OH								1	++
2'-hydroxyflavone						-OH						1	−
3'-hydroxyflavone							-OH					1	−
4'-hydroxyflavone								-OH				1	−
5,3'-dihydroxyflavone		-OH					-OH					1	−
7,3'-dihydroxyflavone				-OH			-OH					1	−
Acacetin		-OH		-OH				-OCH₃				1	−
Apigenin		-OH		-OH				-OH				1	+++
7,4'-dihydroxyflavone				-OH				-OH				1	+
5,4'-dihydroxyflavone		-OH						-OH				1	−
Scutellarein		-OH	-OH	-OH				-OH				1	−
Luteolin		-OH		-OH			-OH	-OH				1	+++
Tricetin		-OH		-OH			-OH	-OH	-OH			1	−
Naringenin		-OH		-OH				-OH				0	−
Kaempferol		-OH		-OH				-OH			-OH	1	−
Morin		-OH		-OH		-OH		-OH			-OH	1	−
Quercetin		-OH		-OH			-OH	-OH			-OH	1	−
Myricetin		-OH		-OH			-OH	-OH	-OH		-OH	1	−

Figure 1. Activity of Compounds with Flavone Skeleton Examined for mRNA Processing Inhibition
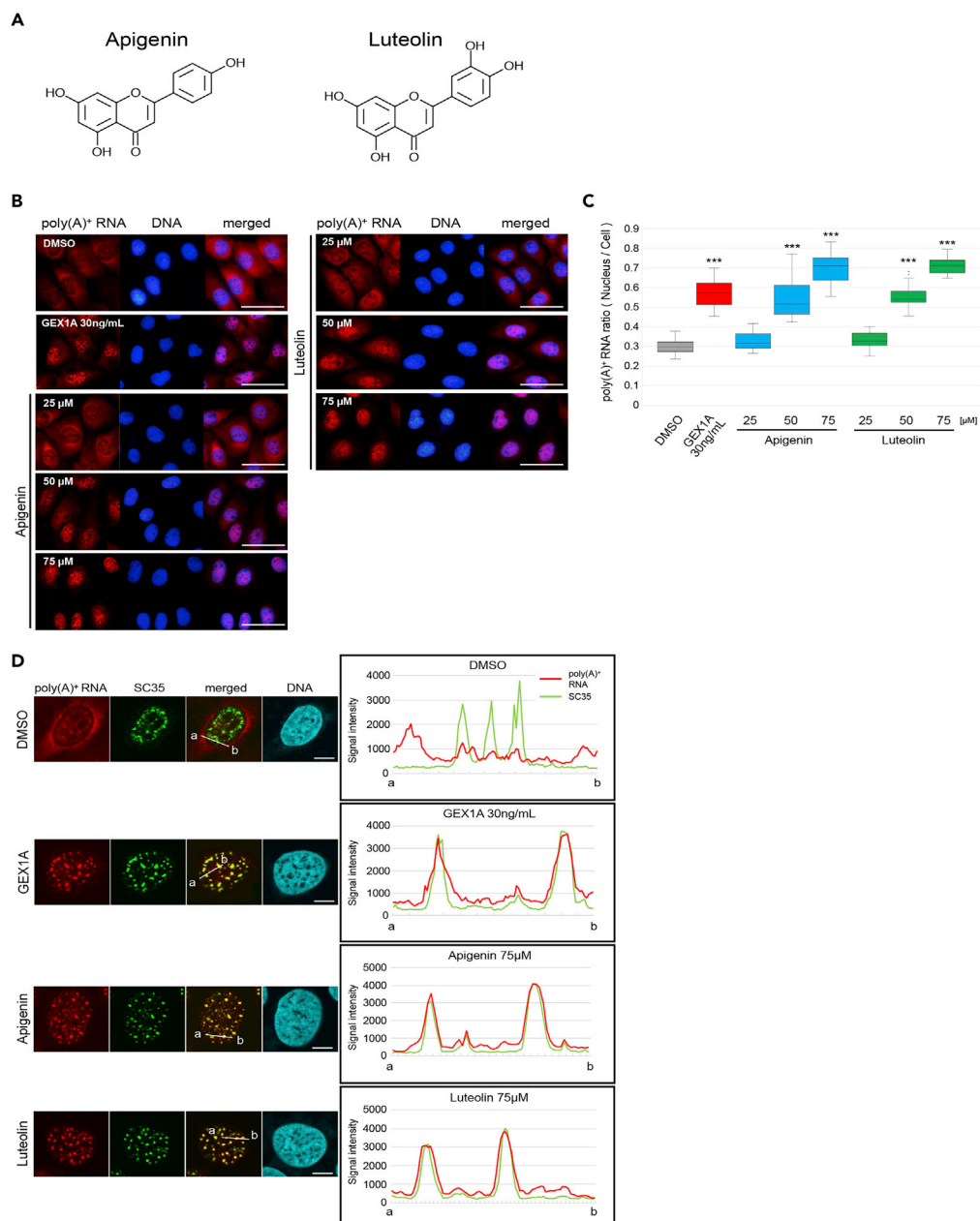See also Figure S1.

Figure 2. Inhibitory Activity against mRNA Processing of Apigenin and Luteolin

(A) Chemical structures of apigenin and luteolin.

(B) RNA-FISH was performed to determine the localization of bulk poly(A)+ RNA. U2OS cells were treated with the indicated concentrations of each compound for 24 h GEX1A (30 ng/mL) was used as a positive control. The bulk poly(A)+ RNA was visualized by Alexa Fluor 594-labeled oligo-dT$_{45}$ probe. The nuclei were visualized with DAPI. Scale bar, 50 μm.

(C) The ratio of the nuclear distribution of mRNA was analyzed. The signal intensities of the whole cell and the nucleus were quantified using ImageJ (n = 35). Boxes show median (center line) and upper and lower quartiles. Whiskers show the lowest and highest values. Statistical analysis was performed using one-way ANOVA followed by Dunnett's test. ***p < 0.001.

(D) The localization of bulk poly(A)+ RNA and nuclear speckles. Poly(A)+ RNA (red), speckles (green), and chromosomal DNA (blue) were visualized in U2OS cells for co-localization analysis. Cells were treated with each indicated compound for 24 h. Scale bar, 10 μm. In right panels, signal intensities of poly(A)+ RNA and SC35 were plotted between a and b lines in the left panels. Poly(A)+ RNA and SC35 signal are shown with red and green lines, respectively.
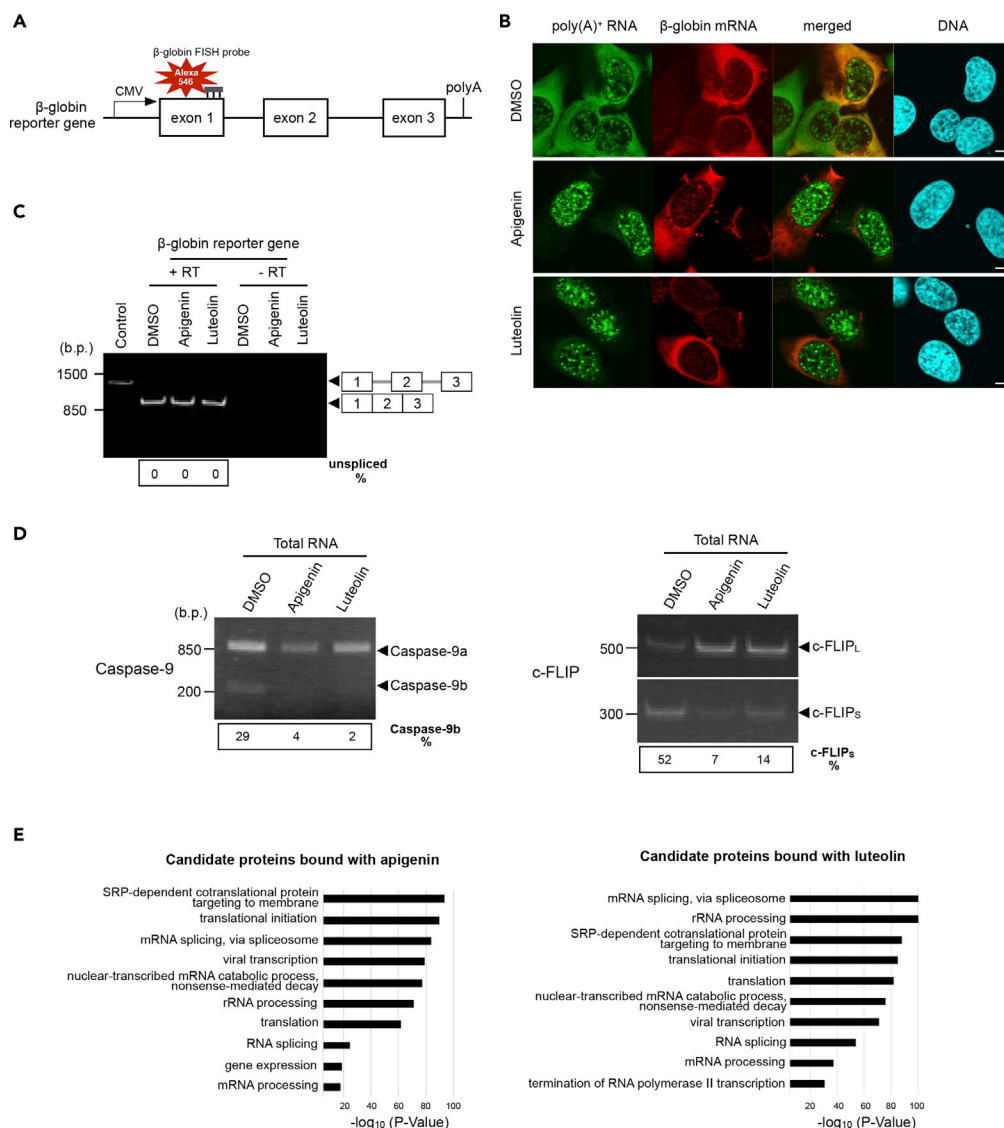
See also Figure S2.

Figure 3. The Effect on Splicing of Some Genes and Identification of Apigenin- and Luteolin-Targeted Proteins

(A) Schematic of *β-globin* construct containing the CMV promoter and BGH poly(A) site is presented. Horizontal lines indicate introns, and boxes indicate exons.

(B) The localization of *β-globin* mRNA was observed. Bulk poly(A)$^+$ RNA (green), *β-globin* mRNA (red), and chromosomal DNA (blue) were visualized in U2OS cells. Scale bar, 10 μm.

(C) The splicing pattern of *β-globin* gene was observed by RT-PCR using total RNA. The digit panel below the photo shows the percentage of unspliced mRNA band intensity and representative results of triplicate experiments. DNA size in base pairs (b.p.) is indicated on the left side. Control: marker for unspliced *β-globin* mRNA. RT: reverse transcription.

(D) The change of splicing pattern of *Caspase-9* and *c-FLIP*. RT-PCR was performed using total RNA. DNA size in base pairs (b.p.) is indicated on the right side. The digit panels below the photo show the percentage of the indicated isoform and representative results of triplicate experiments.

(E) Gene ontology analysis of proteins bound with apigenin or luteolin is shown. Proteins with protein score >0 in Tables S1 and S2 were uploaded to the DAVID database for GO analysis.

See also Figures S2–S4.

(Figure S2A), and was distinguishable from the uniform poly(A)$^+$ RNA accumulation throughout the nucleus observed in cells depleted of TAP (also known as NXF1), an mRNA exporter (Figure S2B) (Wang et al., 2018). The subnuclear localization of accumulated poly(A)$^+$ RNA observed in apigenin- and luteolin-treated cells was also reminiscent of a phenotype exhibited by cells treated with spliceostatin A, a well-known splicing

inhibitor, also implicating the mRNA splicing process as a cellular target of these flavonoids (Figure 2D) (Carvalho et al., 2017; Kaida et al., 2007).

To explore the way in which these flavonoids influence poly(A)$^+$ RNA metabolism in human cells, proteins bound to apigenin and luteolin were analyzed. Flavonoid was fixed on magnetic FG beads with an epoxy linker and was incubated with nuclear extract from HEK293 cells. Purified proteins were analyzed by LC-MS/MS (Figures 3E, S3A, and S3B; Tables S1 and S2). The interaction between some of the LC-MS/MS-detected proteins and either apigenin or luteolin was confirmed by the western blotting using specific antibodies against these proteins (Figure S3C). Gene ontology analysis demonstrated that many of the detected proteins have mRNA splicing-related functions (Figure 3E). Further detailed classification of the splicing-related proteins according to a previous report indicated that these compounds most intensely interact with U2 and U5 snRNP, components of the spliceosome (Figure S3B) (Hegele et al., 2012). HNRNPA2B1, a protein that has been reported to interact with apigenin (Arango et al., 2013), was also detected to a lesser extent than U2 and U5 snRNP components. To obtain insights into the interaction of apigenin and luteolin with their potential targets, docking studies were performed using the crystal structure of human SF3B1, a component of the SF3B subcomplex in the U2 snRNP, in a complex with E7107, a pladienolide derivative analog (PDB code: 5ZYA) (Finci et al., 2018). Our docking algorithm predicted that apigenin and luteolin are likely to bind to SF3B1 near the E7107-binding site (Figure S4A). Both flavonoids interact with several hydrophobic residues such as Leu1066, Val1114, Val1110, and Lys1067, which are also key residues for the hydrophobic interactions between E7107 and SF3B1 (Figure S4B). In addition, the overexpression of SF3B1 attenuated the nuclear accumulation of poly(A)$^+$ RNA induced by the apigenin- and luteolin-treatment (Figure S4C). These results provide evidence that SF3B1 is one of the cellular targets for apigenin and luteolin and plays a crucial role in the modulation of mRNA splicing by these flavonoids.

Taking these findings together, apigenin and luteolin bind to spliceosome components, and in the cells treated with these compounds, changes in the splicing of at least some mRNAs can be effectively induced, whereas the splicing of other mRNAs, such as the *β-globin* mRNA reporter, is less influenced. These findings imply that apigenin and luteolin affect the splicing of a subset of introns, rather than generally inhibiting splicing reactions.

Apigenin and Luteolin Treatment Causes Numerous Alternative Splicing Events

To elucidate the effect of these flavonoids on mRNA splicing, we compared the poly(A)$^+$ RNA profile in flavonoid-treated cells with that in control cells using RNA-seq. Poly(A)$^+$ RNA was purified from total RNAs derived from either control cells or flavonoid-treated cells. RNA-seq reads were mapped with STAR (Dobin et al., 2013) against the hg38 human genome and to the obtained mapping data; we applied rMATS, a bioinformatic tool, to detect alternative splicing events (Figure 4A) (Shen et al., 2014). We detected a wide variety of alternative splicing events induced by treatment with either flavonoid (Figures 4B and 4C). Among the altered splicing patterns, retained intron (RI) was the most frequently detected, followed by skipped exon (SE). Since apigenin and luteolin have similar structures and binding proteins, we hypothesized that they commonly regulate mRNA splicing. To investigate the regulatory mechanism involved, we focused on their common events (Figures 4D and S5). Specifically, we performed gene ontology analysis on the events overlapping between apigenin- and luteolin-treated cells (Figures 4E and S5), indicating that the mRNAs with the retention of introns due to these flavonoids are particularly associated with RNA processing, mRNA metabolic process, and mRNA splicing. RT-PCR using cDNA generated from total RNA successfully confirmed some of the apigenin- and luteolin-derived RIs and another alternative splicing event identified in our rMATS analysis, whereas neither tricetin nor naringenin induced these changes. This demonstrated the significance of the specific structure within these flavonoids for their ability to exert such activity (Figures 4F and S6). Previous studies suggested that unspliced mRNAs are inefficiently exported to the cytoplasm, leading to poly(A)$^+$ RNA accumulation in nuclear speckles (Johnson et al., 2000; Kaida et al., 2007). Based on these findings, we hypothesized that a phenotype derived from apigenin and luteolin treatment, namely, the nuclear speckle-associated poly(A)$^+$ RNA accumulation, reflects nuclear-retained mRNAs with introns. Therefore, we focused on the RIs for further investigation.

Apigenin- and Luteolin-Induced Alternative Splicing Leads to a Change in Gene Expression

Taking into account the possibility that mRNAs with RIs are less effectively exported to the cytoplasm, it was assumed that the expression of genes with apigenin- and luteolin-sensitive introns decreases upon
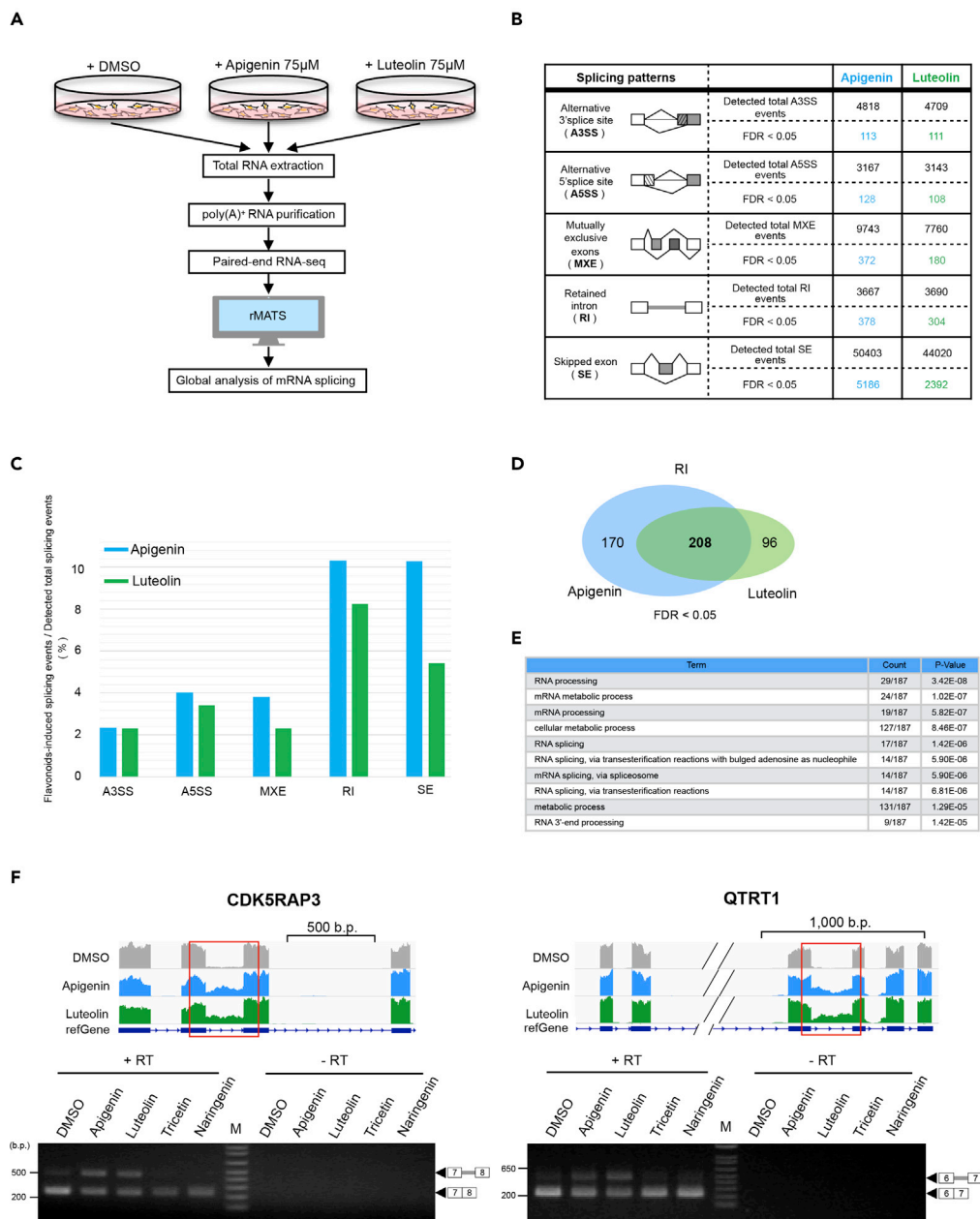
Figure 4. Global Analysis of mRNA Splicing Affected by Apigenin and Luteolin

(A) Alternative splicing analysis scheme. Cells were treated with DMSO, apigenin (75 μM), or luteolin (75 μM) for 24 h; then, total RNA was extracted from the cells. Next, poly(A)$^+$ RNA was purified and fragmented for RNA sequencing. Alternative splicing analysis was performed using rMATS.

(B) Alternative splicing analysis revealed five alternative splicing patterns that were output by rMATS. Upper row indicates the numbers of total splicing events detected in each alternative splicing pattern; bottom row indicates the numbers of statistically significant (false discovery rate: FDR <0.05) splicing pattern changes upon apigenin (blue) or luteolin treatment (green).

(C) Frequency of splicing pattern changes by apigenin or luteolin relative to the total splicing events is calculated using the data in (B).

(D) Venn diagram shows the numbers of apigenin- or luteolin-induced retained intron events.

(E) Gene ontology analysis of apigenin- and luteolin-induced retained intron events. Common target genes of apigenin and luteolin (the number shown in bold in Figure 4D) were uploaded to the DAVID database for GO analysis. Apigenin- and luteolin-targeted genes in U2OS cells were enriched for several GO terms categorized in "Biological Process." Ten GO terms are listed in order of their p values. The "Count" column denominator indicates the number of genes assigned a

Figure 4. *Continued*

DAVID ID among the uploaded target genes of apigenin and luteolin in retained intron events. The numerator indicates the number of genes associated with each GO term.

(F) Validation of retained introns regulated by apigenin and luteolin. In the upper panels, IGV snapshots of retained introns induced by apigenin (blue) and luteolin (green) are shown. Gene structure is depicted at the bottom of each snapshot, with horizontal lines indicating introns and boxes indicating exons. Red square lines surrounding introns indicate regions affected by apigenin and luteolin. Lower panels: RT-PCR was performed using total RNA samples to detect apigenin- or luteolin-induced retained introns. Representative results of triplicate experiments are shown. DNA size in base pairs (b.p.) is indicated on the left side. RT: reverse transcription. M: DNA size marker.

See also Figures S5 and S6.

treatment with these flavonoids. To test this hypothesis, we fractionated the cytoplasmic RNA (Figure S7A). Our RT-PCR analysis clearly detected RIs caused by the treatment with these flavonoids in the whole-cell fractions, but not in the cytoplasmic fractions, indicating that mRNAs harboring those introns are not exported to and/or eliminated in the cytoplasm (Figure 5A). A significant decrease in the expression of genes whose splicing is inhibited by apigenin and luteolin treatment was demonstrated for the matured mRNAs in the cytoplasm (Figure 5A), as well as at the protein level (ANKZF1, PSMA1, and ZWINT) (Figure S7B). In contrast, SEs triggered by apigenin and luteolin treatment were efficiently detected in either fraction (Figure S7C), indicating that these mRNAs associated with exon skipping are efficiently exported to the cytoplasm. Neither the splicing nor the cytoplasmic expression level of nontarget introns appeared to be affected following treatment with apigenin and luteolin.

Intron retention often produces premature termination codon (PTC) that makes the associated coding mRNAs sensitive to nonsense-mediated mRNA decay (NMD) in the cytoplasm (Ge and Porse, 2014). Indeed, we found PTCs within apigenin- and luteolin-derived unspliced mRNAs (Figure 5B). The absence of these unspliced mRNAs in the cytoplasm might be explained by the intense susceptibility of these RNAs to NMD, besides the retention of RNAs within the nucleus. To discriminate between these two possibilities, an NMD assay was performed (Figure 5B). In the cytoplasmic fraction, a PTC-containing transcript variant of *SRSF2*, a well-known NMD target (Feng et al., 2015), was detected only in the presence of cycloheximide (CHX), an NMD inhibitor, demonstrating disturbed NMD under these conditions. In contrast, unspliced mRNAs caused by apigenin and luteolin were not detected irrespective of the integrity of NMD, indicating that apigenin- and luteolin-elicited unspliced mRNAs are eliminated from the cytoplasm mainly by their nuclear retention, rather than by the digestion in the cytoplasm.

Taking these findings together, as a consequence of various alternative splicing events, such as the nuclear retention of unspliced mRNAs and the expression of exon skipping-caused transcript variants, these flavonoids induce a change in the cytoplasmic transcriptome.

Apigenin and Luteolin Inhibit Splicing of Introns with Weak Splice Sites

To characterize introns whose splicing is affected by apigenin and luteolin, we compared their intron length, GC content, splice site score, and BPS score with those of all of the introns annotated in the human genome (Figure 6A). Splice site score was calculated using MaxEntScan (Yeo and Burge, 2004). The BPS score was calculated using the SVM-BP program (Corvelo et al., 2010). The results suggested that RIs caused by apigenin and luteolin treatment are shorter, have weaker 5' and 3' splice sites, and show higher GC content, whereas the BPS scores are similar between these flavonoid-target and nontarget introns.

To confirm the significance of weak splice sites for the susceptibility to these flavonoids, sequences of 5' and 3' splice sites within introns of interest were manipulated to display a higher splice site score, and it was examined whether the splicing of these engineered introns is still sensitive to apigenin and luteolin. For this purpose, introns accompanied by portions of both neighboring exons were cloned into an expression vector, and these vectors were transiently transfected into U2OS cells, achieving the expression of these reporter RNAs under the control of the CMV promoter. We successfully obtained several mini genes, *PLXNB1*, *PSMA1*, and *ANKZF1*, which can efficiently reproduce apigenin- and luteolin-induced intron retention exhibited by the endogenous genes (Figure 5A). Mutating the splice sites of the introns in these mini genes to raise the splice sites with a higher score, namely, changes of $1.11 \rightarrow 6.99$ or $1.11 \rightarrow 9.46$ in the 3' splice site score (3' ss score) of the *PLXNB1* mini gene, $-5.12 \rightarrow 9.07$ in the 5' splice site score (5' ss score), $-9.15 \rightarrow 9.66$ in the 3' ss score in the *PSMA1* mini gene, and $-0.11 \rightarrow 10.45$ in the 5' ss score in the *ANKZF1* mini gene, almost abolished their responses to apigenin and luteolin (Figures 6B, 6C, and S8). In addition,
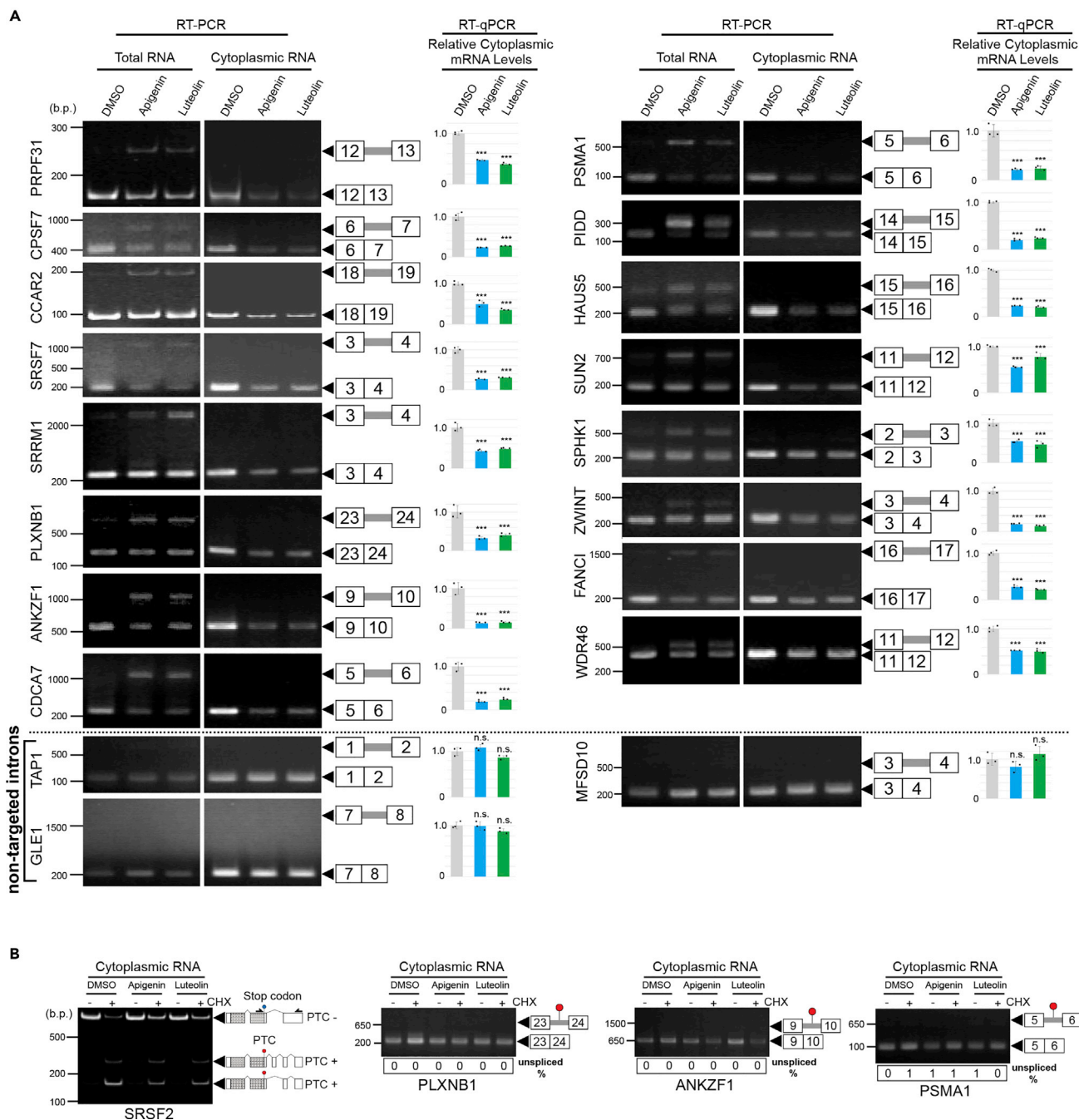
Figure 5. The Expression Level of Retained Intron-Containing mRNA in the Cytoplasm

(A) Detection of retained intron events in the cytoplasm after apigenin and luteolin treatment. RT-PCR was performed using total RNA and cytoplasmic RNA. DNA size in base pairs (b.p.) is indicated on the left side. Non-targeted introns that are not regulated by apigenin and luteolin are shown at the bottom of (A). Representative results of triplicate experiments are shown. To compare the mRNA expression in cytoplasmic fractions, RT-qPCR was performed using cytoplasmic RNA. Values represent the relative expression of the indicated mRNA normalized to *TBP*. Each value is mean ± SD of three independent experiments. Statistical analysis was performed using one-way ANOVA followed by Dunnett's test. ***p < 0.001, n.s.: not significant.

(B) The effect of nonsense-mediated decay (NMD) on mRNA with retained intron in the cytoplasmic fraction was examined. Cycloheximide (CHX) was used as an NMD inhibitor. U2OS cells were treated with CHX (50 μg/mL) in the presence of apigenin (75 μM) or luteolin (75 μM) for 24 h. RT-PCR products of variant transcripts were detected. The digit panels below the photo shows the percentage of unspliced mRNA band intensity and representative results of triplicate experiments. Blue circle indicates a reference stop codon, and red circle indicates a premature termination codon (PTC). PTC + means that the transcript variant has PTC. *SRSF2*, a well-known target of NMD, was used as a positive control (Feng et al., 2015). Dotted region in the *SRSF2* figure indicates protein-coding sequence, and primer locations (black arrows) are marked on the *SRSF2* gene.
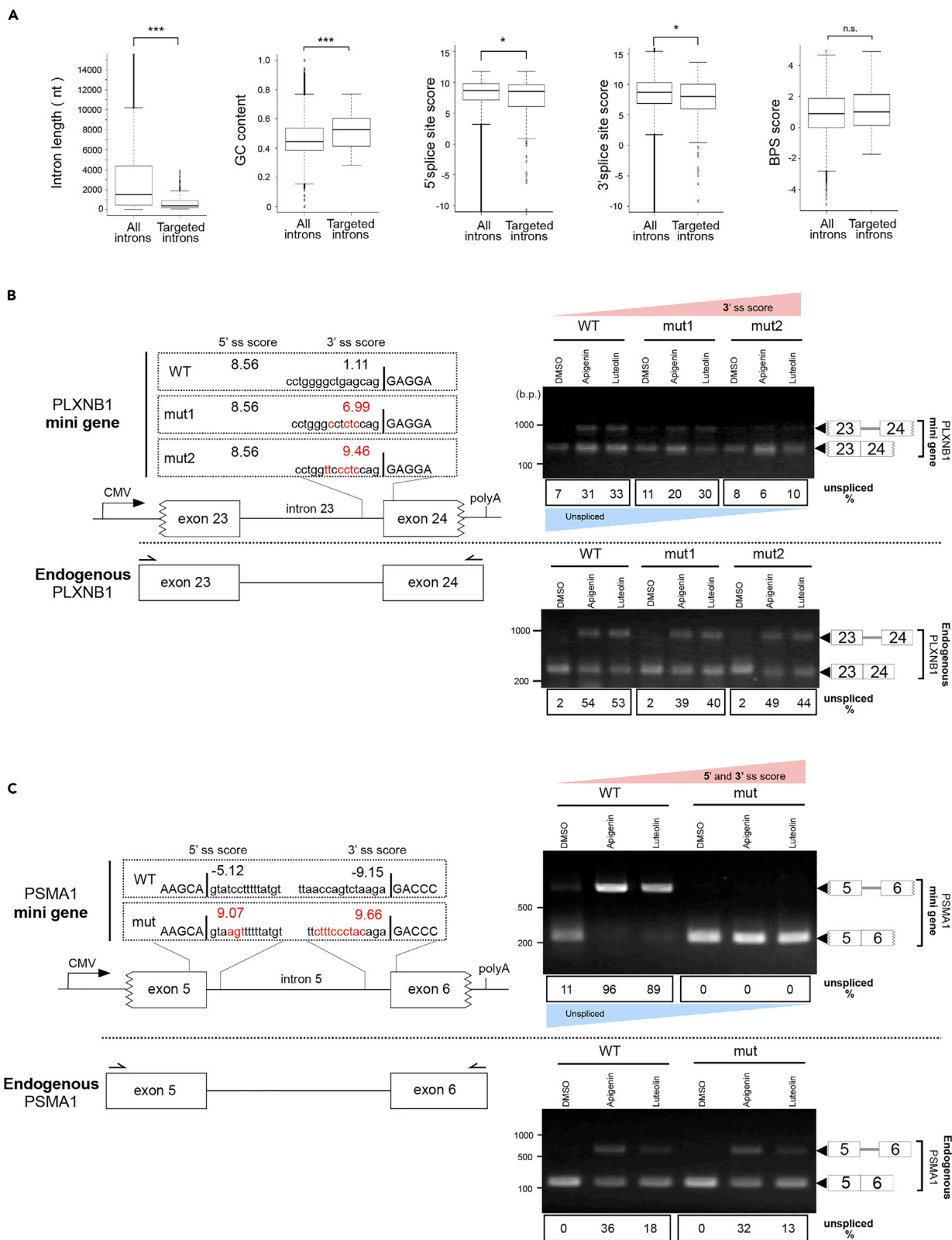
See also Figure S7.

Figure 6. Apigenin and Luteolin Induce Intron Retention with Weak Splice Sites

(A) The bioinformatic analysis on retained introns induced by apigenin and luteolin. All introns of human reference genes and retained introns induced by apigenin and luteolin were analyzed. Boxes show median (center line) and upper and lower quartile ranges. Whiskers show the lowest and highest values. Statistical analysis was performed using the two-sided Mann–Whitney U test. *p < 0.05, ***p < 0.001, n.s.: not significant.

(B and C) Upper left panels in (B and C) present schematic representations of mini gene constructs affected by apigenin and luteolin. The CMV promoter and BGH poly(A) sites are shown. Jagged line in the figure of the exon indicates that the edges of the exons have been partially deleted in order to distinguish endogenous mRNA from transgene-derived mRNA. The mutated nucleotides in each mutated-mini gene construct are shown in red, and the exon sequence is shown in upper case. Splice site score (ss score) was calculated using MaxEntScan. Lower left panels in (B and C) present schematic representations of the endogenous gene. The locations of the primers that amplify the endogenous target are marked in the schematic representation of the endogenous gene (black arrows). Right panels in (B and C) show the results of RT-PCR. DNA size in base pairs (b.p.) is indicated on the left side. The mRNAs derived from the transgene are shown in the upper right panels, and endogenous mRNAs are shown in the lower right panels. The digit panels below the photo show the percentage of unspliced mRNA band intensity and representative results of triplicate experiments.

See also Figure S8.

the *PLXNB1* mini gene with its 3′ ss mutated to achieve a moderate score of 6.99 still exhibited subtle susceptibility to these flavonoids. The efficiencies of either apigenin or luteolin treatment in these experiments were confirmed by RT-PCR analysis of the endogenous mRNAs from the same samples transiently expressing each reporter mini gene (Figures 6B, 6C, and S8). And as mentioned above, the *β-globin* reporter indicated that its transcript escaped from flavonoid-induced splicing inhibition (Figures 3B and 3C). These findings suggest that weak splice sites are crucial for an intron's susceptibility to apigenin and luteolin.

Apigenin- and Luteolin-Derived Unspliced mRNAs Accumulate at Nuclear Speckles

Next, we assessed the subcellular localization of these mini gene-derived mRNAs in the presence or absence of apigenin and luteolin to examine whether the nuclear accumulation of bulk poly(A)$^+$ RNAs observed in the flavonoid-treated cells contains the flavonoid-caused unspliced mRNAs. To visualize these reporter mRNAs, a sequence complementary to the *β-globin* FISH probe used as shown in Figure 3A was inserted into either the *PLXNB1* or *PSMA1* mini gene. RT-PCR analysis demonstrated that *β-globin* sequence-fused mini genes maintained their response to the flavonoids (Figure 7A). The results also showed that mutating the splice sites to have a higher score abolished their response to the flavonoids, as observed with native sequence reporters (Figures 6B, 6C, and 7A). In either apigenin-/luteolin-treated or untreated cells, these mini genes were transiently expressed and visualized by FISH using *β-globin* probe (Figure 7B). Bulk poly(A)$^+$ RNA was simultaneously visualized in the same cells to verify the effect of the treatment with flavonoids. In DMSO-treated cells, expressed reporter mRNAs were efficiently exported to the cytoplasm. In apigenin- and luteolin-treated cells, WT reporter mRNAs were diminished from the cytoplasm and accumulated in the nucleus, whereas apigenin- and luteolin-insensitive mutated mRNAs were efficiently exported to the cytoplasm under these conditions. Notably, in the flavonoid-treated nucleus, WT mRNA reporters co-localized with bulk poly(A)$^+$ RNAs, indicating that flavonoid-caused unspliced reporter mRNAs accumulate at the nuclear speckles.

Tumorigenic Cells Exhibit More Prominent Sensitivity to Apigenin and Luteolin than Non-tumorigenic Cells

It has been shown that cancer cells are more sensitive to reagents inhibiting splicing (see Discussion) (Dvinge et al., 2016). We thus assessed whether this is also the case with apigenin and luteolin by comparing their effects on U2OS, HeLa, and MCF7 tumorigenic cell lines with those on non-tumorigenic HaCaT cells. When added at 75 μM, apigenin and luteolin caused prominent nuclear poly(A)$^+$ RNA accumulation in all of the tumorigenic cell lines tested, whereas the nuclear poly(A)$^+$ RNA accumulation in HaCaT cells under the same conditions was moderate (Figure 8A). In addition, tumorigenic cells exhibited a steeper dose response than HaCaT cells.

We also examined the effect of these compounds on the cell viability (Figures 8B and S9). These flavonoids significantly inhibited the proliferation of U2OS cells in a dose- and time-dependent manner. HaCaT cells also exhibited a dose- and time-dependent response to these flavonoids but to a lesser extent than U2OS cells at all doses and time points. Other non-tumorigenic cells, WI-38 and TIG-1, also gave similar results with HaCaT cells. Taken together, apigenin and luteolin seem to be more effective for tumorigenic cells than for non-tumorigenic cells (Figure S9).
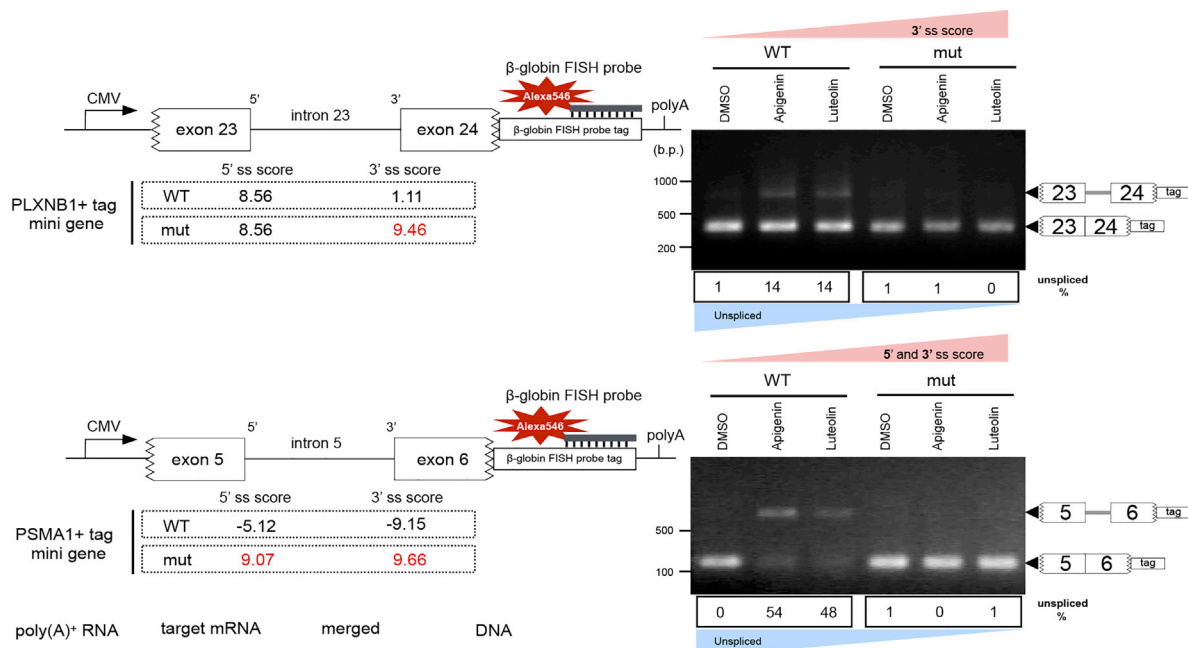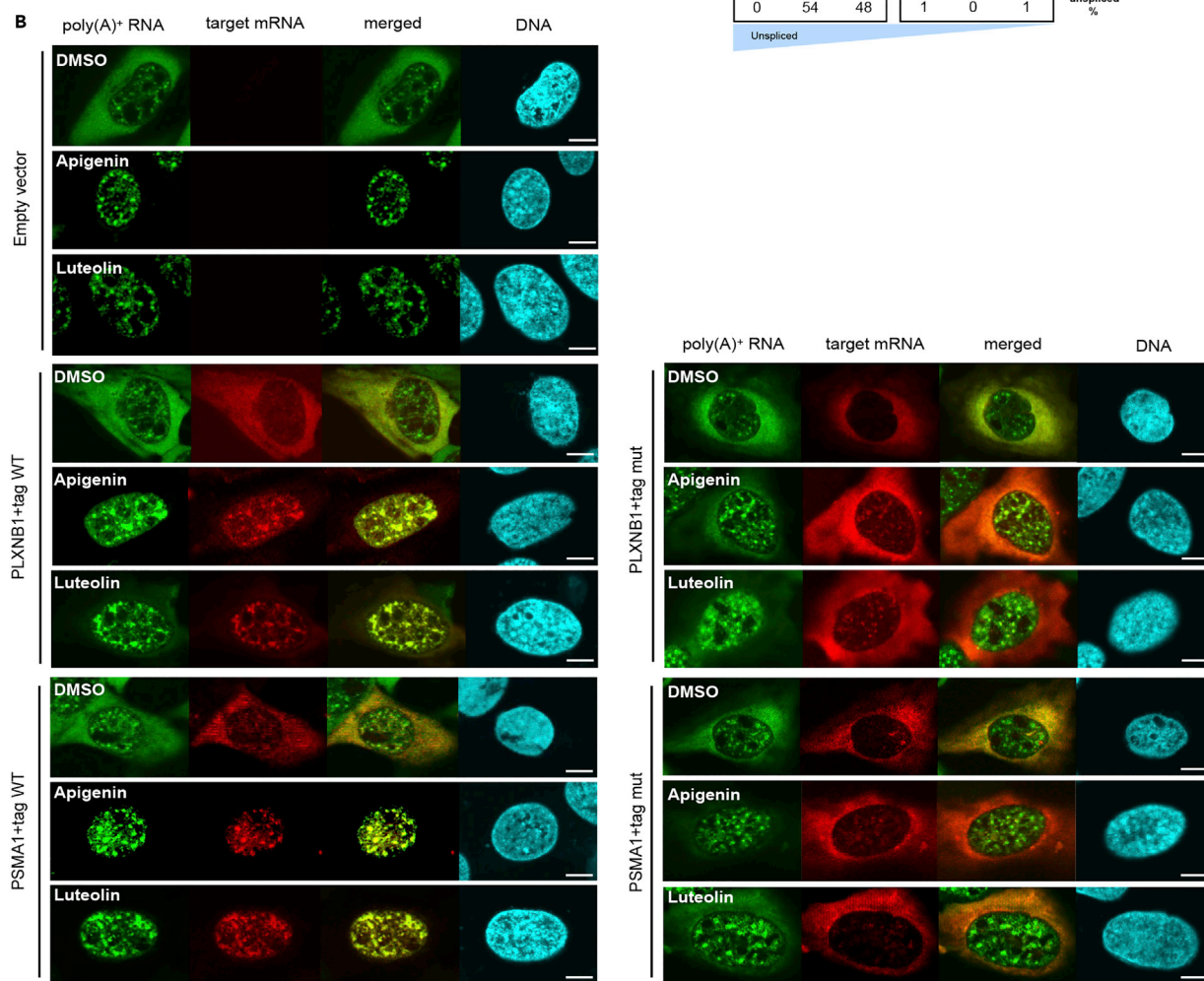
Figure 7. Localization of mRNAs with Retained Intron Induced by Apigenin and Luteolin

(A) Schematic of mini gene constructs with *β-globin* FISH probe tag. The CMV promoter and BGH poly(A) sites are shown. DNA size in base pairs (b.p.) is indicated on the left side. The digit panels below the photo show the percentage of unspliced mRNA band intensity and representative results of triplicate experiments.

(B) The localization of target mRNA was observed. Bulk poly(A)$^+$ RNA (green), target mRNA (red), and chromosomal DNA (blue) were visualized in U2OS cells. Scale bar, 10 μm.

DISCUSSION

Food not only provides nutrition, taste, and texture but also regulates biological function. The daily intake of bioactive food compounds is expected to be effective for the prevention of chronic diseases. For example, polyphenols and carotenoids have antioxidant activity and function in preventing lifestyle-related diseases (Pandey and Rizvi, 2009; Reinisalo et al., 2015; Young and Lowe, 2001). Flavonoids, which are abundant in fruit and vegetables, have been reported to reduce the risk of lifestyle-related diseases and carcinogenesis (Bo et al., 2016; López-lázaro, 2009). Despite the broad bioactivity of flavonoids, few studies on their regulatory activity against mRNA processing, especially splicing, have been reported. We previously searched for compounds derived from food that have the ability to inhibit mRNA processing and identified such effects in compounds with a flavone skeleton (Kurata et al., 2016, 2017).

In this study, we have shown that, among the flavonoids, apigenin and luteolin have remarkable activity of inhibiting mRNA processing. Several lines of evidence indicate that this activity is derived from the direct inhibition of splicing. Our rMATS analysis demonstrated that all types of alternative splicing events are provoked by treatment with apigenin and luteolin, and the retention of introns is the event having the highest frequency. It was previously shown that splicing inhibition by either spliceostatin A treatment or the knockdown of a component of U2 snRNP or U5 snRNP, such as SF3B1 or PRPF8, causes the retention of numerous introns in mRNAs coding RNA processing factors (Wickramasinghe et al., 2015; Yoshimoto et al., 2016), implying that these mRNAs are highly sensitive to splicing inhibition. Such enrichment of RNA processing factors, especially of mRNA splicing, was also observed in the genes that we identified to harbor introns whose retention was induced by apigenin and luteolin. It has been reported that unspliced mRNAs resulting from the global inhibition of splicing by spliceostatin A treatment manifest as a robust accumulation of bulk poly(A)$^+$ RNAs at the nuclear speckles (Carvalho et al., 2017; Kaida et al., 2007). Similarly, we observed that apigenin and luteolin treatment induced the accumulation of bulk poly(A)$^+$ RNA, as well as the retention of intron-containing transcripts from target mini genes, in the nuclear speckles, implying that these flavonoids affect a broad range of mRNA splicing events. Our results from LC-MS/MS, docking studies and SF3B1 overexpression analysis simply suggest that these flavonoids interact with U2 and U5 snRNP, possibly through the interaction with SF3B1, to modulate mRNA splicing, although we cannot exclude other possible splicing regulatory mechanisms by these flavonoids, such as SUMOylation of spliceosomal components previously reported for an apigenin- and luteolin-related biflavonoid, hinokiflavone (Pawellek et al., 2017). Together, these findings suggest that apigenin and luteolin associate with spliceosomal components to directly prevent the function of spliceosomes, thus affecting alternative splicing at the genome-wide level.

Our rMATS analysis did not detect previously demonstrated alternative splicing events induced by apigenin and luteolin treatment, such as the change of splicing pattern of *Caspase-9* and *c-FLIP* mRNA (Arango et al., 2013), although it was efficiently recapitulated by RT-PCR analysis, indicating that these flavonoids actually affect a broader range of splicing events beyond our criteria of rMATS analysis. Such events may include the very subtle splicing perturbation that, if it occurs to numerous targets, can contribute to the flavonoid-induced nuclear bulk poly(A)$^+$ RNA accumulation.

Our data also illustrated a mechanism by which these flavonoids inhibit splicing. The bioinformatic analysis raises the possibility that weak splice sites are a general feature for the retention of introns caused by apigenin and luteolin. Supporting this hypothesis, manipulating the splice site score in the target introns abolished their sensitivity to these flavonoids and led them to be spliced out. Therefore, apigenin and luteolin presumably perturb the association of splicing-related factors with the weak splice sites to inhibit splicing.

We observed more sensitivity of tumorigenic cells to apigenin and luteolin than that observed for non-tumorigenic cells, both for the bulk mRNA processing and cell viability. The exact relationship between

A
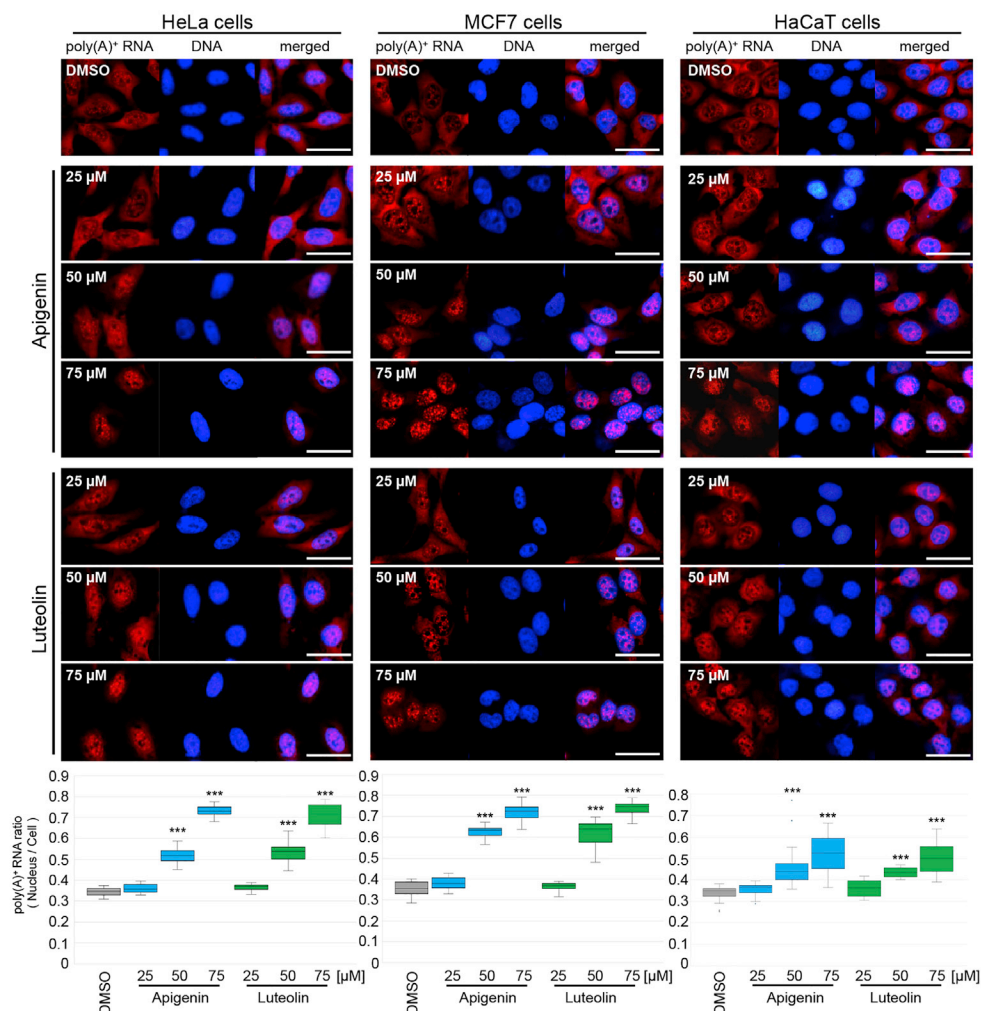
B

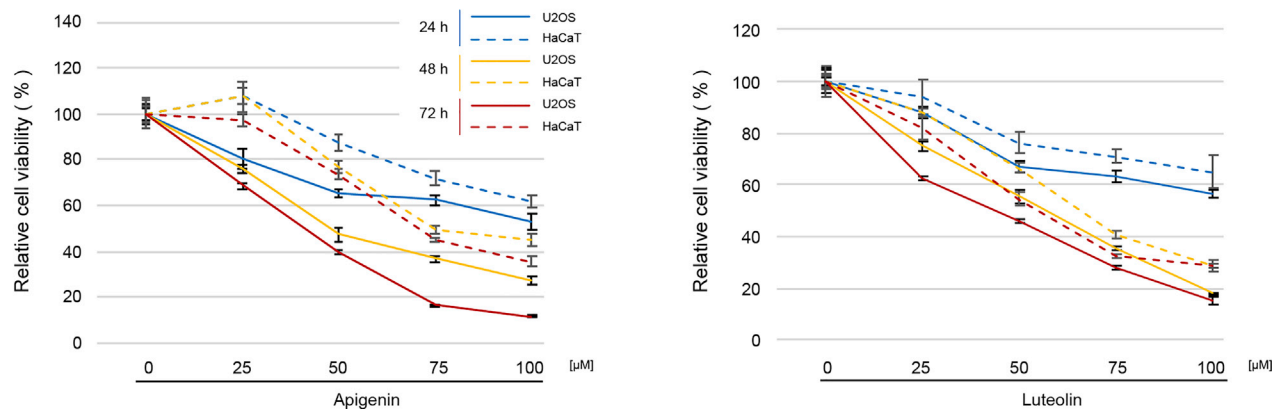**Figure 8. Inhibition of mRNA Processing and Proliferation of Tumorigenic Cells by Apigenin and Luteolin**

(A) Bulk poly(A)$^+$ RNA (red) and chromosomal DNA (blue) were visualized in HeLa, MCF7, and HaCaT cells. Cells were treated with the indicated concentrations of each compound for 24 h. Scale bar, 50 μm. In lower panels, the signal intensities of bulk poly(A)$^+$ RNA in the whole cell and in the nucleus

Figure 8. *Continued*

were quantified using ImageJ (n = 35). Boxes show median (center line) and upper and lower quartiles. Whiskers show the lowest and highest values. Statistical analysis was performed using one-way ANOVA followed by Dunnett's test. ***p < 0.001.

(B) Proliferation of U2OS and HaCaT cells treated with the indicated concentrations of each compound for 24, 48, or 72 h. Cell viability was determined by MTT assay. Cell viability in comparison with that of DMSO-treated cells, which was set to 100%, is reported as mean ± SD of six independent experiments. See also Figure S9.

splicing and cancer progression is still unclear. However, splicing abnormality has been found to be involved in the onset and progression of various cancers (Scotti and Swanson, 2016; Sveen et al., 2016), and it has been suggested that cancers harboring mutations in splicing factors are highly susceptible to splicing inhibition (Lee et al., 2016). For example, acute myeloid leukemia cells with *SF3B1* mutation exhibit reduced viability in the presence of a splicing inhibitor (Seiler et al., 2018). High sensitivity to splicing inhibition has also been demonstrated for cancers caused by *c-Myc* oncogene overexpression (Hsu et al., 2015). In this case, it has been suggested that massive amounts of *c-Myc*-driven pre-mRNA sequester a substantial population of spliceosomes to weaken the splicing activity available for endogenous pre-mRNAs, thus conferring on cells similar sensitivity for splicing inhibition as observed in cancer cells resulting from mutations in splicing factors. Hence, splicing inhibitors are attractive candidates for anti-cancer drugs. Indeed, splicing inhibitors such as H3B-8800 (Seiler et al., 2018) are under clinical trials for anti-cancer therapy. Because the concentrations at which apigenin and luteolin can effectively exert their splicing-inhibiting activities are much higher than those of previously identified compounds, such as spliceostatin A and H3B-8800, the employment of these flavonoids as anti-cancer drugs may not be so promising. Nonetheless, further evaluation of these flavonoids as anti-cancer drugs should be conducted. On the other hand, it has been reported that xenograft progression of human tumors was repressed by the oral administration of apigenin or luteolin into nude mice (Li et al., 2018; Shukla et al., 2015; Xu et al., 2018) and that the daily intake of bulk flavonoids reduced carcinogenesis in humans (Bo et al., 2016; López-lázaro, 2009). These findings suggest a beneficial effect of these compounds on preventing cancer development when they are consumed in food on a daily basis for a considerable period.

Many screening systems to identify anti-cancer compounds are highly focused on finding compounds with strong activity. Therefore, compounds with moderate activity have been overlooked. Our study provides an effective strategy to discover compounds harboring moderate inhibitory activity on mRNA processing and to elucidate the mechanism underlying the disruption of mRNA processing induced by candidate compounds.

Limitations of the Study

We have revealed the underlying mechanism that food-derived compounds apigenin and luteolin cause intron retention. Other than intron retention, we also observed various alternative splicing events induced by these flavonoids and whether an analogous molecular mechanism contributes to these events remains to be assessed.

A hypersensitivity of cancer cells to the splicing inhibition has been shown in many studies, implying our observed *in vitro* inhibition of cancer cell proliferation by apigenin and luteolin, as well as the previously demonstrated suppression of human tumor xenograft progression by apigenin-treatment in a mouse model, is derived from the inhibited splicing. However, a further investigation should be required to elucidate a direct relationship between these flavonoids' inhibitory activity on splicing and their exhibited tumor growth suppressive effect.

METHODS

All methods can be found in the accompanying Transparent Methods supplemental file.

DATA AND CODE AVAILABILITY

The RNA-seq data were submitted to Gene Expression Omnibus (accession number: GSE128097). Original imaging data have been deposited to Mendeley Data and are available at https://doi.org/10.17632/t6r9jftdnr.1.

SUPPLEMENTAL INFORMATION

Supplemental Information can be found online at https://doi.org/10.1016/j.isci.2019.11.033.

AUTHOR CONTRIBUTIONS

M.K., Y.S., and S.M. conceived the study; M.K. and Y.Y. conducted biological experiments; H.K. and N.T. performed RNA-seq; M.K., N.F., K.F., and S.S. performed bioinformatic analysis; Y.M. performed docking studies; M.K. and S.S. performed statistical analysis; and M.K., N.F., K.F., and S.M. analyzed the results and wrote the paper. All authors reviewed the final manuscript.

DECLARATION OF INTERESTS

The authors declare no competing interests.

REFERENCES

Arango, D., Morohashi, K., Yilmaz, A., Kuramochi, K., Parihar, A., Brahimaj, B., Grotewold, E., and Doseff, A.I. (2013). Molecular basis for the action of a dietary flavonoid revealed by the comprehensive identification of apigenin human targets. Proc. Natl. Acad. Sci. U S A *110*, E2153–E2162.

Bo, Y., Sun, J., Wang, M., Ding, J., Lu, Q., and Yuan, L. (2016). Dietary flavonoid intake and the risk of digestive tract cancers: a systematic review and meta-analysis. Sci. Rep. *6*, 1–8.

Carvalho, T., Martins, S., Rino, J., Marinho, S., and Carmo-Fonseca, M. (2017). Pharmacological inhibition of the spliceosome subunit SF3b triggers exon junction complex-independent nonsense-mediated decay. J. Cell Sci. *130*, 1519–1531.

Corvelo, A., Hallegger, M., Smith, C.W.J., and Eyras, E. (2010). Genome-wide association between branch point properties and alternative splicing. PLoS Comput. Biol. *6*, e1001016.

Daguenet, E., Dujardin, G., and Valcarcel, J. (2015). The pathogenicity of splicing defects: mechanistic insights into pre-mRNA processing inform novel therapeutic approaches. EMBO Rep. *16*, 1640–1655.

Dobin, A., Davis, C.A., Schlesinger, F., Drenkow, J., Zaleski, C., Jha, S., Batut, P., Chaisson, M., and Gingeras, T.R. (2013). STAR: ultrafast universal RNA-seq aligner. Bioinformatics *29*, 15–21.

Dvinge, H., Kim, E., Abdel-Wahab, O., and Bradley, R.K. (2016). RNA splicing factors as oncoproteins and tumour suppressors. Nat. Rev. Cancer *16*, 413–430.

Effenberger, K.A., Urabe, V.K., and Jurica, M.S. (2017). Modulating splicing with small molecular inhibitors of the spliceosome. Wiley Interdiscip. Rev. RNA *8*, e1381.

Feng, D., Su, R.C., Zou, L., Triggs-Raine, B., Huang, S., and Xie, J. (2015). Increase of a group of PTC+ transcripts by curcumin through inhibition of the NMD pathway. Biochim. Biophys. Acta *1849*, 1104–1115.

Finci, L.I., Zhang, X., Huang, X., Zhou, Q., Tsai, J., Teng, T., Agrawal, A., Chan, B., Irwin, S., Karr, C., et al. (2018). The cryo-EM structure of the SF3b spliceosome complex bound to a splicing modulator reveals a pre-mRNA substrate competitive mechanism of action. Genes Dev. *32*, 309–320.

Fujita, K., Okamura, M., Nishimoto, S., Kurihara, T., Momma, K., Miyamae, Y., Kambe, T., Nagao, M., Narita, H., and Masuda, S. (2012). Establishment of a monitoring system to detect inhibition of mRNA processing. Biosci. Biotechnol. Biochem. *76*, 1248–1251.

Fujiwara, N., Yoshikawa, M., Yamazaki, T., Kambe, T., Nagao, M., and Masuda, S. (2010). A screening method tuned for mRNA processing factors in human cells by evaluation of the luciferase reporter activity and the subcellular distribution of bulk poly(A)+ RNA. Biosci. Biotechnol. Biochem. *74*, 1512–1516.

Ge, Y., and Porse, B.T. (2014). The functional consequences of intron retention: alternative splicing coupled to NMD as a regulator of gene expression. BioEssays *36*, 236–243.

Hahn, C.N., Venugopal, P., Scott, H.S., and Hiwase, D.K. (2015). Splice factor mutations and alternative splicing as drivers of hematopoietic malignancy. Immunol. Rev. *263*, 257–278.

Hasegawa, M., Miura, T., Kuzuya, K., Inoue, A., Ki, S.W., Horinouchi, S., Yoshida, T., Kunoh, T., Koseki, K., Mino, K., et al. (2011). Identification of SAP155 as the target of GEX1A (Herboxidiene), an antitumor natural product. ACS Chem. Biol. *6*, 229–233.

Hegele, A., Kamburov, A., Grossmann, A., Sourlis, C., Wowro, S., Weimann, M., Will, C.L., Pena, V., Lührmann, R., and Stelzl, U. (2012). Dynamic protein-protein interaction wiring of the human spliceosome. Mol. Cell *45*, 567–580.

Hoskins, A.A., and Moore, M.J. (2012). The spliceosome: a flexible, reversible macromolecular machine. Trends Biochem. Sci. *37*, 179–188.

Hsu, T.Y.T., Simon, L.M., Neill, N.J., Marcotte, R., Sayad, A., Bland, C.S., Echeverria, G.V., Sun, T., Kurley, S.J., Tyagi, S., et al. (2015). The

spliceosome is a therapeutic vulnerability in MYC-driven cancer. Nature 525, 384–388.

Johnson, C., Primorac, D., McKinstry, M., McNeil, J., Rowe, D., and Lawrence, J.B. (2000). Tracking COL1A1 RNA in osteogenesis imperfecta: splice-defective transcripts initiate transport from the gene but are retained within the SC35 domain. J. Cell Biol. 150, 417–431.

Kaida, D., Motoyoshi, H., Tashiro, E., Nojima, T., Hagiwara, M., Ishigami, K., Watanabe, H., Kitahara, T., Yoshida, T., Nakajima, H., et al. (2007). Spliceostatin A targets SF3b and inhibits both splicing and nuclear retention of pre-mRNA. Nat. Chem. Biol. 3, 576–583.

Kim, M.S., Pinto, S.M., Getnet, D., Nirujogi, R.S., Manda, S.S., Chaerkady, R., Madugundu, A.K., Kelkar, D.S., Isserlin, R., Jain, S., et al. (2014). A draft map of the human proteome. Nature 509, 575–581.

Kotake, Y., Sagane, K., Owa, T., Mimori-Kiyosue, Y., Shimizu, H., Uesugi, M., Ishihama, Y., Iwata, M., and Mizui, Y. (2007). Splicing factor SF3b as a target of the antitumor natural product pladienolide. Nat. Chem. Biol. 3, 570–575.

Kurata, M., Murata, Y., Momma, K., Fouad Ali Mursi, I., Takahashi, M., Miyamae, Y., Kambe, T., Nagao, M., Narita, H., Shibuya, Y., et al. (2016). The isoflavone fraction from soybean presents mRNA maturation inhibition activity. Biosci. Biotechnol. Biochem. 81, 551–554.

Kurata, M., Morimoto, M., Kawamura, Y., Fouad Ali Mursi, I., Momma, K., Takahashi, M., Miyamae, Y., Kambe, T., Nagao, M., Narita, H., et al. (2017). Inhibition of mRNA maturation by compounds which have a flavonoid skeleton. Biochem. Mol. Biol. 2, 46–53.

Lee, C.S., Dias, A.P., Jedrychowski, M., Patel, A.H., Hsu, J.L., and Reed, R. (2008). Human DDX3 functions in translation and interacts with the translation initiation factor eIF3. Nucleic Acids Res. 36, 4708–4718.

Lee, S.C.W., Dvinge, H., Kim, E., Cho, H., Micol, J.B., Chung, Y.R., Durham, B.H., Yoshimi, A., Kim, Y.J., Thomas, M., et al. (2016). Modulation of splicing catalysis for therapeutic targeting of leukemia with mutations in genes encoding spliceosomal proteins. Nat. Med. 22, 672–692.

Li, Z., Zhang, Y., Chen, L., and Li, H. (2018). The dietary compound luteolin inhibits pancreatic cancer growth by targeting BCL-2. Food Funct. 9, 3018–3027.

López-lázaro, M. (2009). Distribution and biological activities of the flavonoid luteolin. Mini Rev. Med. Chem. 9, 31–59.

Maguire, S.L., Leonidou, A., Wai, P., Marchiò, C., Ng, C.K., Sapino, A., Salomon, A.V., Reis-Filho, J.S., Weigelt, B., and Natrajan, R.C. (2015). SF3B1 mutations constitute a novel therapeutic target in breast cancer. J. Pathol. 235, 571–580.

Maniatis, T., and Reed, R. (2002). An extensive network of coupling among gene expression machines. Nature 416, 499–506.

Markus, M.A., Marques, F.Z., and Morris, B.J. (2011). Resveratrol, by modulating RNA processing factor levels, can influence the alternative splicing of Pre-mRNAs. PLoS One 6, e28926.

Millevoi, S., and Vagner, S. (2009). Molecular mechanisms of eukaryotic pre-mRNA 3' end processing regulation. Nucleic Acids Res. 38, 2757–2774.

Nlend Nlend, R., Meyer, K., and Schümperli, D. (2010). Repair of pre-mRNA splicing: prospects for a therapy for spinal muscular atrophy. RNA Biol. 7, 430–440.

Orphanides, G., and Reinberg, D. (2002). A unified theory of gene expression. Cell 108, 439–451.

Pan, Q., Shai, O., Lee, L.J., Frey, B.J., and Blencowe, B.J. (2008). Deep surveying of alternative splicing complexity in the human transcriptome by high-throughput sequencing. Nat. Genet. 40, 1413–1415.

Pandey, K.B., and Rizvi, S.I. (2009). Plant polyphenols as dietary antioxidants in human health and disease. Oxid. Med. Cell. Longev. 2, 270–278.

Pawellek, A., Ryder, U., Tammsalu, T., King, L.J., Kreinin, H., Ly, T., Hay, R.T., Hartley, R.C., and Lamond, A.I. (2017). Characterisation of the biflavonoid hinokiflavone as a pre-mRNA splicing modulator that inhibits SENP. Elife 6, e27402.

Reinisalo, M., Kårlund, A., Koskela, A., Kaarniranta, K., and Karjalainen, R.O. (2015). Polyphenol stilbenes: molecular mechanisms of defence against oxidative stress and aging-related diseases. Oxid. Med. Cell. Longev. 2015, 1–24.

Sakla, M.S., and Lorson, C.L. (2008). Induction of full-length survival motor neuron by polyphenol botanical compounds. Hum. Genet. 122, 635–643.

Salton, M., and Misteli, T. (2016). Small molecule modulators of pre-mRNA splicing in cancer therapy. Trends Mol. Med. 22, 28–37.

Scotti, M.M., and Swanson, M.S. (2016). RNA mis-splicing in disease. Nat. Rev. Genet. 17, 19–32.

Seiler, M., Yoshimi, A., Darman, R., Chan, B., Keaney, G., Thomas, M., Agrawal, A.A., Caleb, B., Csibi, A., Sean, E., et al. (2018). H3B-8800, an orally available small-molecule splicing modulator, induces lethality in spliceosome-mutant cancers. Nat. Med. 24, 497–504.

Shen, S., Park, J.W., Lu, Z., Lin, L., Henry, M.D., Wu, Y.N., Zhou, Q., and Xing, Y. (2014). rMATS: robust and flexible detection of differential alternative splicing from replicate RNA-Seq data. Proc. Natl. Acad. Sci. U S A 111, E5593–E5601.

Shukla, S., Kanwal, R., Shankar, E., Datt, M., Chance, M.R., Fu, P., MacLennan, G.T., and Gupta, S. (2015). Apigenin blocks IKKα activation and suppresses prostate cancer progression. Oncotarget 6, 31216–31232.

Sveen, A., Kilpinen, S., Ruusulehto, A., Lothe, R.A., and Skotheim, R.I. (2016). Aberrant RNA splicing in cancer; Expression changes and driver mutations of splicing factor genes. Oncogene 35, 2413–2427.

Wahl, M.C., and Lührmann, R. (2015). SnapShot: spliceosome dynamics III. Cell 162, 690.

Wang, E.T., Sandberg, R., Luo, S., Khrebtukova, I., Zhang, L., Mayr, C., Kingsmore, S.F., Schroth, G.P., and Burge, C.B. (2008). Alternative isoform regulation in human tissue transcriptomes. Nature 456, 470–476.

Wang, K., Wang, L., Wang, J., Chen, S., Shi, M., and Cheng, H. (2018). Intronless mRNAs transit through nuclear speckles to gain export competence. J. Cell Biol. 217, 3912–3929.

Wickramasinghe, V.O., Gonzàlez-Porta, M., Perera, D., Bartolozzi, A.R., Sibley, C.R., Hallegger, M., Ule, J., Marioni, J.C., and Venkitaraman, A.R. (2015). Regulation of constitutive and alternative mRNA splicing across the human transcriptome by PRPF8 is determined by 5' splice site strength. Genome Biol. 16, 1–21.

Xu, L., Zhang, Y., Tian, K., Chen, X., Zhang, R., Mu, X., Wu, Y., Wang, D., Wang, S., Liu, F., et al. (2018). Apigenin suppresses PD-L1 expression in melanoma and host dendritic cells to elicit synergistic therapeutic effects. J. Exp. Clin. Cancer Res. 37, 1–15.

Yeo, G., and Burge, C.B. (2004). Maximum entropy modeling of short sequence motifs with applications to RNA splicing signals. J. Comput. Biol. 11, 377–394.

Yoshida, K., Sanada, M., Shiraishi, Y., Nowak, D., Nagata, Y., Yamamoto, R., Sato, Y., Sato-Otsubo, A., Kon, A., Nagasaki, M., et al. (2011). Frequent pathway mutations of splicing machinery in myelodysplasia. Nature 478, 64–69.

Yoshimoto, R., Kaida, D., Furuno, M., Maxwell, B.A., Noma, S., Suzuki, H., Kawamura, Y., Hayashizaki, Y., Mayeda, A., and Yoshida, M. (2016). Global analysis of pre-mRNA subcellular localization following splicing inhibition by spliceostatin A. RNA 23, 47–57.

Young, A.J., and Lowe, G.M. (2001). Antioxidant and prooxidant properties of carotenoids. Arch. Biochem. Biophys. 385, 20–27.

Supplemental Information

Food-Derived Compounds Apigenin and Luteolin

Modulate mRNA Splicing of Introns

with Weak Splice Sites

Masashi Kurata, Naoko Fujiwara, Ken-ichi Fujita, Yasutaka Yamanaka, Shigeto Seno, Hisato Kobayashi, Yusaku Miyamae, Nobuyuki Takahashi, Yasuyuki Shibuya, and Seiji Masuda
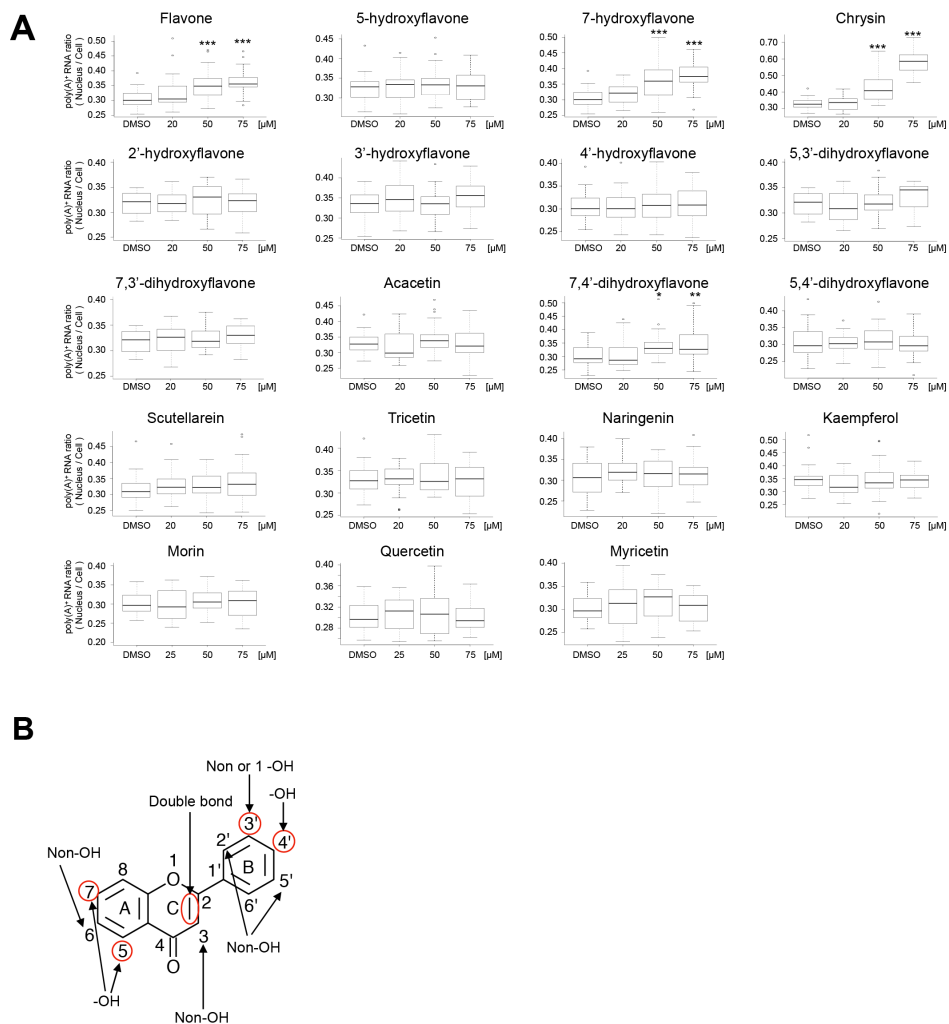
Figure S1. Accumulation of poly(A)$^+$ RNA by the indicated chemical compounds with a flavone skeleton. (Related to Figure 1)

(A) mRNA processing inhibitory activity of chemical compounds with a flavone skeleton. The ratio of nuclear distribution of mRNA is shown. The signal intensities of bulk poly(A)$^+$ RNA in the whole-cell and in the nucleus were quantified using ImageJ (n = 35). Boxes show median (center line) and upper and lower quartiles. Whiskers show the lowest and highest values. Statistical analysis was performed using one-way ANOVA followed by Dunnett's test. *p < 0.05, **p < 0.01, ***p < 0.001.

(B) Chemical structure with strong mRNA processing inhibitory activity.
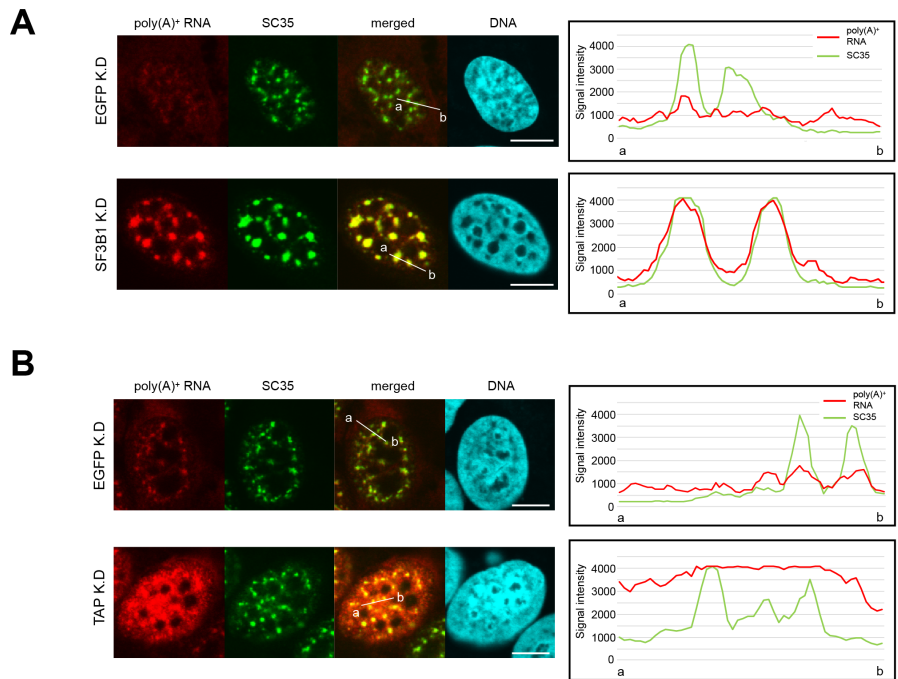
Figure S2. Localization of poly(A)$^+$ RNA in cells depleted of splicing factor, SF3B1, and mRNA exporter, TAP. (Related to Figures 2 and 3)

(A) and (B)   Localization of poly(A)$^+$ RNA in U2OS cells. Poly(A)$^+$ RNA localization (red) was observed in SF3B1 (A) and TAP (B) knockdown conditions. SC35 (green) was used to stain the nuclear speckle. DAPI (blue) was used to visualize the nuclei. Scale bar, 10 μm. In right panels, signal intensities of poly(A)$^+$ RNA and SC35 were plotted between a and b lines in the left panels.

A

B

C

HEK293 cells

U2OS cells
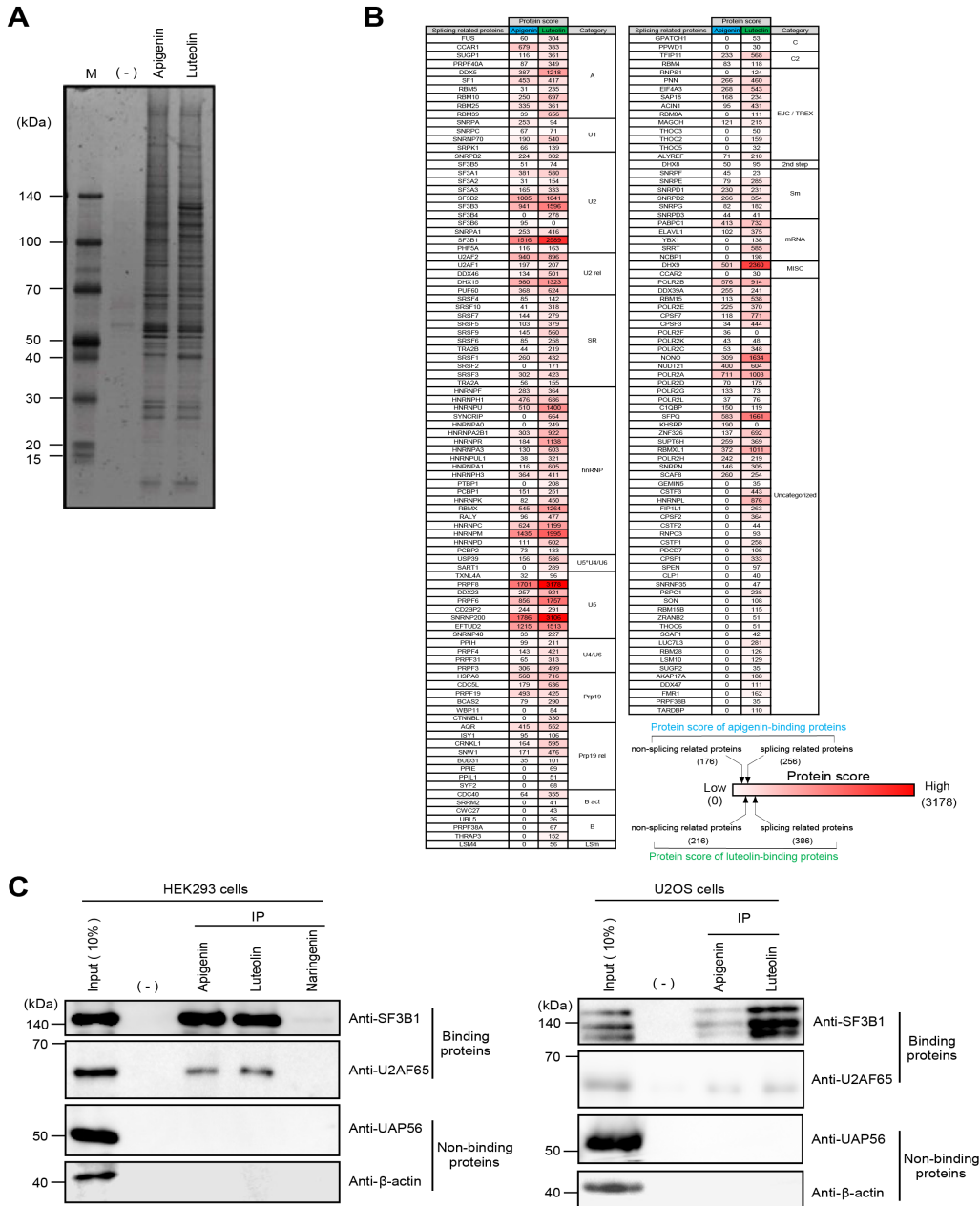
Figure S3. Detection of apigenin- and luteolin-binding proteins. (Related to Figure 3)

(A) Apigenin- and luteolin-binding proteins were purified from the nuclear extracts of HEK293 cells with unfixed (−) or flavonoid-fixed FG beads and were analyzed by silver staining. The binding proteins were analyzed by LC-MS/MS. M: Protein size marker.

(B) Splicing-related proteins binding to apigenin or luteolin. Prot_scores of control and apigenin- and luteolin-target proteins in Tables S1 and S2 were calculated using Mascot software (Matrix Science). Protein score is obtained by subtracting the prot_score of the control from that of apigenin or luteolin. Splicing-related proteins with protein score > 0 were extracted. When multiple protein scores were calculated for one protein, the highest value is listed. In the lower right bar, higher color intensity indicates a higher protein score. "Low" represents the lowest value, and "High" represents the highest value among the protein scores of splicing-related proteins. The black arrow indicates the average value of each protein score.

(C) Apigenin- and luteolin-binding proteins in HEK293 cells (left) and U2OS cells (right) were analyzed by western blotting. Naringenin was used as a negative control. The antibodies are indicated on the right side of each panel.
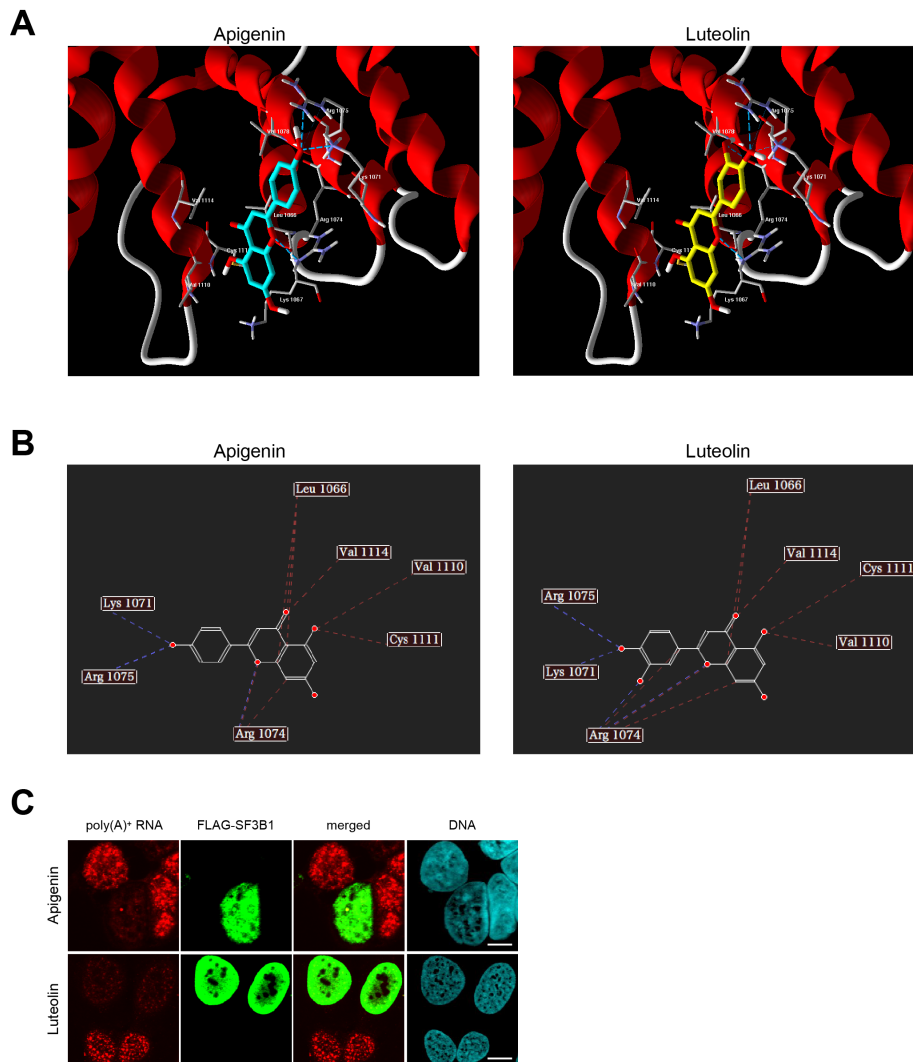
Figure S4. Binding of apigenin and luteolin in SF3B1. (Related to Figure 3)

(A) The crystal structure of human SF3B1 and E7107 was retrieved from the RCSB protein data bank (PDB code 5ZYA). The potential binding site of apigenin and luteolin in the SF3B complex was searched for and detected in the pocket near the branch point adenosine recognition site. The putative binding modes of apigenin and luteolin are displayed in sky blue and yellow, respectively.

(B) The simulation predicted that both apigenin and luteolin interact with several hydrophobic residues such as Leu1066, Val1114, Val1110, and Lys1067 of SF3B1. The Lys1071, Arg1074,

and Arg1075 are also the key residues for the hydrophobic interaction between E7107 and SF3B1, and are located near the BPA recognition site (Finci et al., 2018).

(C) The overexpression of FLAG-SF3B1 attenuated the flavonoid-induced nuclear poly(A)$^+$ RNA accumulation. Poly(A)$^+$ RNA (red), exogenously expressed FLAG-SF3B1 (green), and chromosomal DNA (blue) were visualized in U2OS cells. Scale bar, 10 µm.

A3SS

Apigenin 59 | **54** | Luteolin 57

FDR < 0.05

Term	Count	P-Value
cellular nitrogen compound biosynthetic process	30/52	1.42E-05
RNA metabolic process	28/52	4.75E-05
cellular biosynthetic process	32/52	1.20E-04
transcription from RNA polymerase II promoter	16/52	1.39E-04
cellular nitrogen compound metabolic process	33/52	1.48E-04
organic substance biosynthetic process	32/52	1.75E-04
biosynthetic process	32/52	2.39E-04
organic cyclic compound biosynthetic process	26/52	2.96E-04
nucleic acid metabolic process	28/52	3.30E-04
nucleobase-containing compound metabolic process	30/52	3.51E-04

A5SS

70 | **58** | 50

Term	Count	P-Value
intracellular transport	17/52	1.81E-06
RNA processing	13/52	3.26E-06
establishment of localization in cell	18/52	7.71E-06
mRNA metabolic process	11/52	8.83E-06
cellular localization	19/52	4.57E-05
macromolecule localization	19/52	1.81E-04
cellular macromolecule localization	14/52	2.18E-04
translation	9/52	2.66E-04
organic substance transport	18/52	2.96E-04
peptide biosynthetic process	9/52	3.48E-04

MXE

273 | **99** | 81

Term	Count	P-Value
cellular macromolecule metabolic process	48/75	5.50E-05
macromolecule metabolic process	50/75	9.81E-05
positive regulation of cellular metabolic process	24/75	1.45E-04
positive regulation of metabolic process	25/75	1.55E-04
positive regulation of macromolecule metabolic process	24/75	1.59E-04
regulation of molecular function	24/75	1.65E-04
regulation of protein metabolic process	22/75	2.07E-04
organic substance metabolic process	54/75	3.10E-04
positive regulation of protein metabolic process	16/75	3.62E-04
cellular metabolic process	52/75	4.85E-04

SE

3388 | **1798** | 594

Term	Count	P-Value
organelle organization	361/1199	3.27E-20
cellular nitrogen compound metabolic process	549/1199	5.00E-20
cellular macromolecule metabolic process	662/1199	1.58E-18
nitrogen compound metabolic process	570/1199	3.70E-18
RNA processing	126/1199	1.75E-17
cellular component organization or biogenesis	522/1199	2.66E-17
nucleobase-containing compound metabolic process	486/1199	9.03E-16
heterocycle metabolic process	494/1199	9.60E-16
cellular component organization	504/1199	3.80E-15
cellular metabolic process	758/1199	4.02E-15

Figure S5. Gene ontology analysis of apigenin- and luteolin-induced A3SS, A5SS, MXE, and SE. (Related to Figure 4)

Common target genes of apigenin and luteolin (the number shown in bold) were uploaded to the DAVID database for GO analysis. Apigenin- and luteolin-target genes in U2OS cells were enriched for several GO terms categorized into "Biological Process." Ten GO terms are listed in order of their p values. The denominator of the "Count" column indicates the number of genes assigned a DAVID ID among the uploaded target genes of apigenin and luteolin in each alternative splicing event. The numerator indicates the number of genes involved in each GO term.
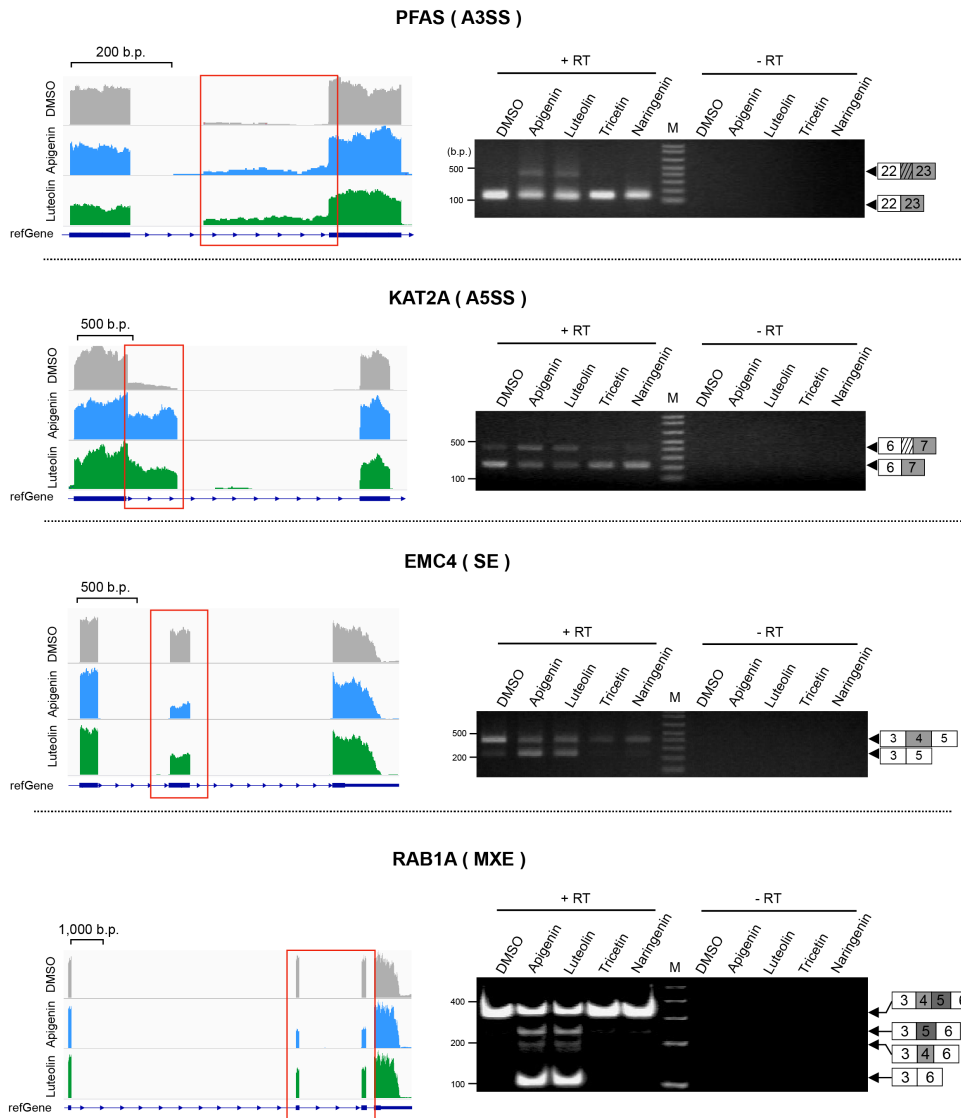
Figure S6. Validation of A3SS, A5SS, SE, and MXE regulated by apigenin and luteolin. (Related to Figure 4)

In the left panels, IGV snapshots of A3SS, A5SS, SE, and MXE induced by apigenin (blue) and luteolin (green) are shown. Gene structure is depicted at the bottom of each snapshot with horizontal lines indicating introns and boxes indicating exons. Red square lines surrounding alternative exons indicate regions affected by apigenin and luteolin. As shown in the right panels, RT-PCR was performed using total RNA samples in order to detect the apigenin- or luteolin-induced alternative splicing change. Representative results of triplicate experiments are shown. DNA size in base pairs (b.p.) is indicated on the left side. RT: reverse transcription. M: DNA size marker.
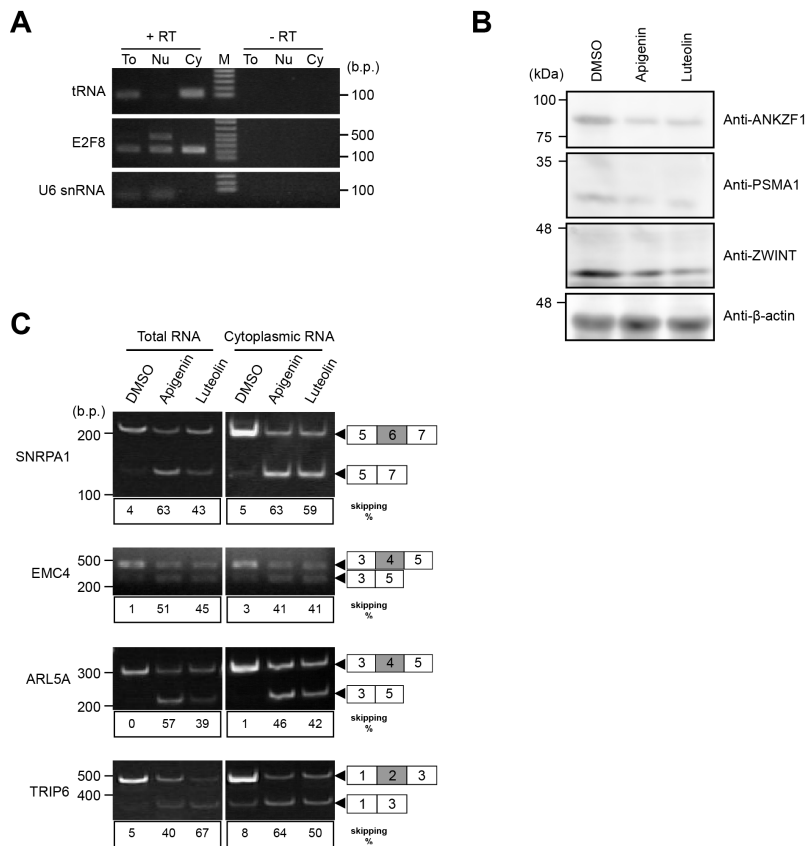
Figure S7. Expression of mRNA with altered splicing pattern in the cytoplasm. (Related to Figure 5)

(A) Fractionation of the nuclear, cytoplasmic, and total RNA was carried out. tRNA was detected as a dominant RNA species in the cytoplasmic fraction. *E2F8* mRNA was used to confirm that the fractionation had been successfully performed. U6 snRNA served as a nuclear marker. DNA size in base pairs (b.p.) is indicated on the right side. To: total RNA, Nu: nuclear RNA, Cy: cytoplasmic RNA. M: DNA size marker. RT: reverse transcription.

(B) Effect of flavonoids on protein expression. The U2OS cells were treated with apigenin or luteolin (75μM) for 24 h. Total cell extracts were subjected to SDS-PAGE and analyzed by Western blotting. Representative blots are shown. The antibodies are indicated on the right side of each panel.

(C) Skipped exon induced by apigenin and luteolin treatment was detected using total RNA and cytoplasmic RNA by RT-PCR. The digit panels below the photo show the percentage of exon skipping band intensity and representative results of triplicate experiments.
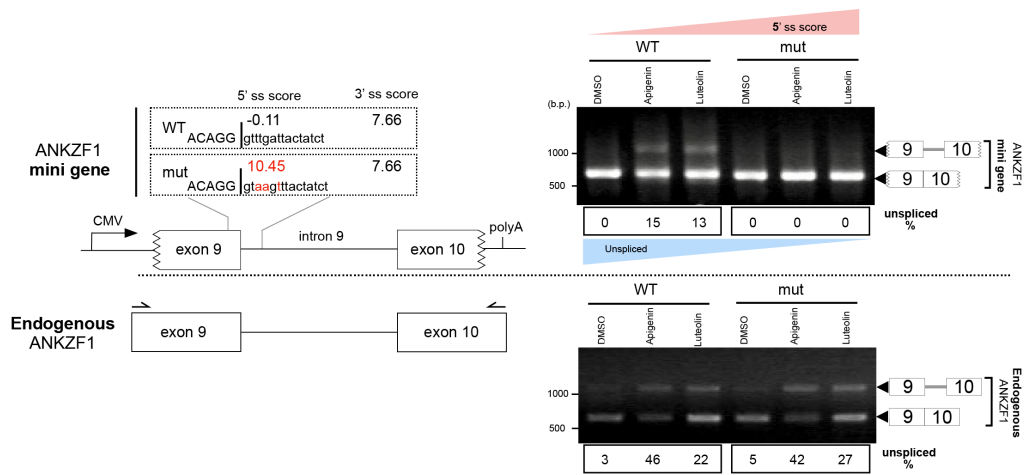
Figure S8. Apigenin and luteolin induce intron retention with weak splice sites. (Related to Figure 6)

The upper left panel presents a schematic representation of mini gene constructs affected by apigenin and luteolin. The CMV promoter and BGH poly(A) sites are shown. Jagged line in the figure of the exon indicates that the edges of the exons have been partially deleted in order to distinguish endogenous mRNA from transgene-derived mRNAs. The mutated nucleotides in each mutated-mini gene construct are shown in red, and the exon sequence is shown in upper case. The splice site (ss) score was calculated using MaxEntScan. The lower left panel presents a schematic representation of the endogenous gene. The locations of the primer that amplify the endogenous target are marked on the schematic representation of the endogenous gene (black arrows). Right panels show the results of RT-PCR. DNA size in base pairs (b.p.) is indicated on the left side. The mRNAs derived from the transgene are shown in the upper right panels, and endogenous mRNAs are shown in the lower right panels. The digit panels below the photo show the percentage of unspliced mRNA band intensity and representative results of triplicate experiments.
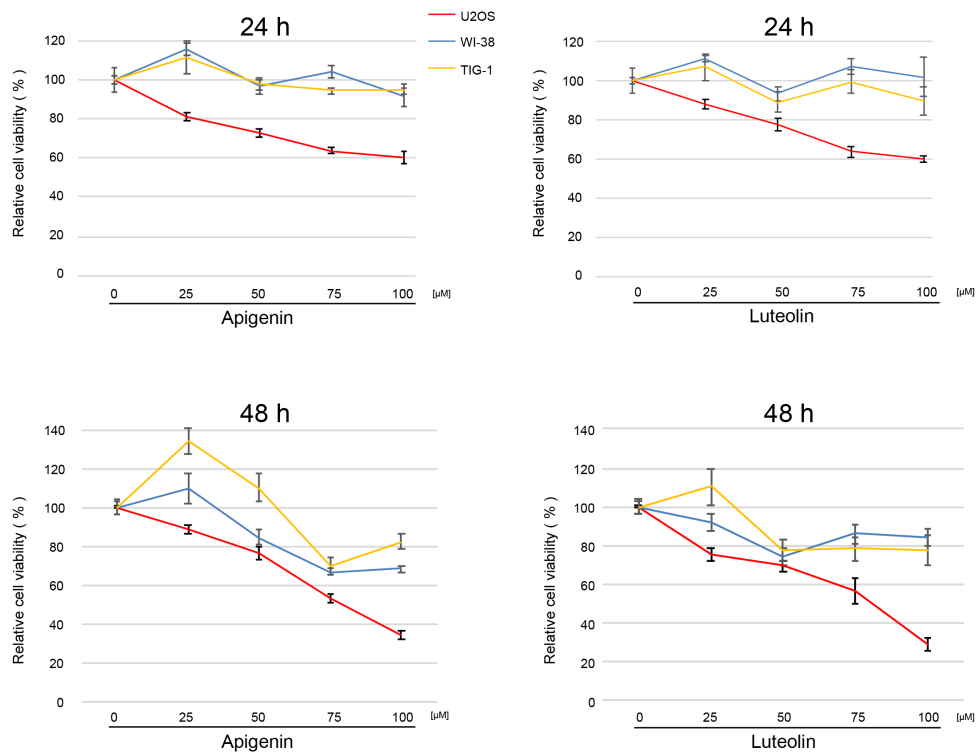
Figure S9. Inhibition of the proliferation in non-tumorigenic cells by apigenin and luteolin. (Related to Figure 8)

The proliferation of non-tumorigenic cells, WI-38 and TIG-1, treated with the indicated concentrations of each compound for 24 or 48 h and compared with that of U2OS cells. Cell viability was determined by MTT assay. Cell viability in comparison with that of DMSO-treated cells, set to 100%, is reported as mean ± SD of six independent experiments.

Table S4. The sequence of siRNAs in this study. (Related to Figures 2 and 3)

Name	Nucleotide sequence	Source
EGFP	GGGCACAAGCUGGAGUACAACUACA	Invitrogen
TAP	GAACUGGUUCAAGAUUACAAUUCCU	Invitrogen

SF3B1 siRNA was predesigned by IDT. The catalog number is hs.Ri.SF3B1.13.1.

TRANSPARENT METHODS

Cell culture

U2OS, HeLa, MCF7, HaCaT, and HEK293 cells were maintained in Dulbecco's Modified Eagle Medium (Wako, Kyoto, Japan) supplemented with 10% heat-inactivated fetal bovine serum at 37°C. WI-38 and TIG-1 cells were maintained in Eagle's minimum essential medium (Wako) supplemented with 10% heat-inactivated fetal bovine serum at 37°C.

Antibodies

The commercial antibodies used were as follows: anti-SF3B1 mouse monoclonal antibody (1:1000 dilution) (a kind gift from Robin Reed, Ph.D.), anti-U2AF65 mouse monoclonal antibody (1:1000 dilution) (also from Robin Reed, Ph.D.), anti-β-actin mouse monoclonal antibody (1:2000 dilution) (Sigma-Aldrich, St. Louis, MO), anti-SC35 mouse monoclonal antibody (1:2000 dilution) (Sigma-Aldrich), anti-FLAG M2 monoclonal antibody (1:1000 dilution) (Sigma-Aldrich), anti-ANKZF1 (1:500 dilution) (GeneTex, Irvine, CA), anti-PSMA1 (1:2000 dilution) (GeneTex), and anti-ZWINT (1:2000 dilution) (GeneTex). Anti-UAP56 rat polyclonal antibody, as described previously, was also used (Yamazaki et al., 2010).

Fluorescence in situ hybridization (RNA-FISH)

Cells (5×10^4 cells/mL) on coverslips in a 12-well plate were cultured for 24 h following inoculation, fixed with 10% formaldehyde in phosphate-buffered saline (PBS) for 20 min, and permeabilized in 0.1% Triton X-100 in PBS for 10 min. Cells were washed three times with PBS for 10 min to remove the detergent, once with 2× standard sodium citrate (SSC) for 5 min to exchange the buffer content, prehybridized with ULTRAhyb-Oligo Hybridization Buffer (Ambion, Austin, TX) for 1 h at 42°C in a humidified chamber, and then incubated overnight with 10 pmol Alexa Fluor 594-labeled oligo-dT$_{45}$ probe (Molecular Probes, Eugene, OR) diluted with hybridization buffer. Cells were washed for 20 min each at 42°C with 2× SSC, 0.5× SSC, and 0.1× SSC. The nuclei were visualized with 4', 6-diamidino-2-phenylindole (DAPI). Fluorescent images were captured at random using a Zeiss Axioplan 2 (Carl Zeiss, Jena, Germany), equipped with an OLYMPUS DP70 camera (OLYMPUS, Tokyo, Japan). Confocal images were obtained by a FLUOVIEW FV10i microscope (OLYMPUS). The ratio of nuclear to total poly(A)$^+$ RNA signals was calculated using ImageJ software

(https://imagej.nih.gov/ij/) (version 1.51w), in accordance with the instructions.

Immunofluorescence

After RNA-FISH, the cells were washed once with PBS and then blocked with 6% bovine serum albumin (BSA) in PBS for 1 h at room temperature. The coverslips were incubated with the primary antibody in PBS containing 2% BSA, followed by secondary antibodies labeled with Alexa Fluor 488. Nuclei were visualized with DAPI.

Preparation of nuclear extracts

HEK293 or U2OS cells were centrifuged, washed twice with PBS, and very carefully suspended in double the pellet volume of hypotonic buffer [10 mM HEPES (pH 7.9), 1.5 mM $MgCl_2$, 10 mM KCl, 0.2 mM phenylmethylsulfonyl fluoride (PMSF), 0.5 mM dithiothreitol (DTT)]. The cells were kept on ice for 10 min, and the cell lysate was obtained by homogenization with a Dounce homogenizer (Wheaton, Millville, NJ). The cell lysate was collected by centrifugation at 13,000×g for 1 min. Half of the pellet volume of low-salt buffer [20 mM HEPES (pH 7.9), 1.5 mM $MgCl_2$, 20 mM KCl, 0.2 mM EDTA, 25% glycerol, 0.2 mM PMSF, 0.5 mM DTT] was then added to the pellet. After suspending the pellet, the same volume of high-salt buffer [20 mM HEPES (pH 7.9), 1.5 mM $MgCl_2$, 1.4 M KCl, 0.2 mM EDTA, 25% glycerol, 0.2 mM PMSF, 0.5 mM DTT] was added dropwise. The cell lysate was gently mixed by rotating at 4°C for 30 min and then centrifuged at 20,000×g for 15 min. The supernatant was collected and dialyzed for 3 h using dialysis buffer [20 mM HEPES (pH 7.9), 100 mM KCl, 0.2 mM EDTA, 20% glycerol, 0.2 mM PMSF, 0.5 mM DTT].

Construction of flavonoid-conjugated beads

Flavonoid was fixed with magnetic FG beads with an epoxy linker (Tamagawa Seiki, Iida, Japan) in the following way. In brief, flavonoid (final concentrations of 10 mM apigenin and 2 mM luteolin) was mixed with 0.5 mg of epoxy beads in N,N-dimethylformamide (DMF) containing K_2CO_3, which included a tenfold molar excess of flavonoid at 37°C overnight, and washed twice with 50% DMF and once with deionized water. Then, the beads were washed three times with 50% methanol (MeOH). The beads were suspended in 50% MeOH and stored at 4°C.

Purification of flavonoid-binding proteins

Flavonoid-fixed or control (unfixed) beads were mixed with HEK293 or U2OS cells nuclear extracts at 4°C for 4 h. After magnetic separation by washing thoroughly with 100 mM KCl buffer [20 mM HEPES-NaOH (pH 7.9), 100 mM KCl, 1 mM $MgCl_2$, 0.2 mM $CaCl_2$, 0.2 mM EDTA, 10% glycerol, 0.1% Nonidet P-40 (NP-40), 1 mM DTT, and 0.2 mM PMSF], the beads were subjected to sodium dodecyl sulfate polyacrylamide gel electrophoresis (SDS-PAGE) analysis and silver staining. To identify the flavonoid-binding proteins, LC-MS/MS analysis was performed by Q Exactive Plus (Thermo Fisher Scientific, Waltham, MA). The outputs of the LC-MS/MS analysis were prot_matches and prot_score. Prot_matches are the numbers of peptides identified (Tables S1 and S2). Prot_score was calculated using Mascot software (Matrix Science, London, UK). Protein scores shown in Figure S3B, and Tables S1 and S2 were calculated by subtracting the prot_score of the control from that of apigenin or luteolin.

Silver staining

The protein samples were mixed with 4× SDS buffer [190 mM Tris-HCl (pH 6.8), 40% glycerol, 0.8% SDS, 0.2% bromophenol blue, and 40 mM DTT] and boiled for 2 min. Protein separation was performed using SuperSep™ Ace, 5%–20%, 17-well (Wako). Silver staining of SDS-PAGE gels was carried out with Silver Staining Kit Protein (GE Healthcare, Little Chalfont, UK), in accordance with the manufacturer's protocol. Pictures were captured using the image analyzer LAS-1000 (Fujifilm, Tokyo, Japan).

Western blotting

Total cell extracts were prepared using RIPA buffer [25 mM Tris-HCl (pH 7.5), 150 mM NaCl, 1% NP-40, 1% sodium deoxycholate, 0.1% SDS, 0.2 mM PMSF and 0.5 mM DTT]. The total cell extracts and nuclear extracts were separated by SDS-PAGE and then electrotransferred to FluoroTrans PVDF Transfer Membranes (Pall, Ann Arbor, MI) using a Bio-Rad Trans-Blot cell (Bio-Rad, Hercules, CA). The blotted PVDF membrane was blocked with 5% skim milk/PBS containing 0.1% Tween 20 for 1 h at room temperature and reacted with the primary antibody with rotation at 4°C overnight. Blots were washed three times with PBS containing 0.1% Tween 20 for 10 min each and then incubated with horseradish peroxidase (HRP)-conjugated secondary antibody with rotation

at room temperature for 2 h. The blotted membranes were washed with PBS containing 0.1% Tween 20 for 10 min three times each, reacted with chemiluminescence reagent (Millipore, Darmstadt, Germany), and detected with the image analyzer LAS 4000 mini (GE Healthcare).

Docking studies

Molecular docking of apigenin and luteolin against the human SF3B1 was carried out using Molegro Virtual Docker ver. 6.0.1 (CLC bio, Aarhus, Denmark). The ligand structures were drawn by Marvin Sketch 5.11.5. The crystal structure of human SF3B1 bound to E7107 was downloaded from RCSB Protein Data Bank (PDB code: 5ZYA) and imported into the docking program according to the software's instructions, by removing all ligands and accessory molecules. Potential ligand-binding sites of proteins were calculated using the Molegro cavity detection algorithm. All parameters were set to default.

Total and cytoplasmic RNA isolation

U2OS cells (20% confluence) treated with or without flavonoids were recovered by trypsinization. Total RNA was isolated by Sepasol-RNA I Super G (Nacalai Tesque, Kyoto, Japan), in accordance with the manufacturer's instructions.

  For cytoplasmic RNA preparation, the cells recovered by trypsinization were treated with lysis buffer [20 mM Tris-HCl (pH 8.0), 200 mM NaCl, 1 mM $MgCl_2$, 1% NP-40] on ice for 5 min. The cytoplasmic fraction was isolated by brief spinning. RNA in the cytoplasmic fraction was isolated by Sepasol-RNA I Super G, in accordance with the manufacturer's instructions.

Reverse transcription-polymerase chain reaction (RT-PCR)

Complementary DNA (cDNA) was synthesized from the extracted RNA using ReverTraAce (Toyobo, Osaka, Japan) and random 9-mer primer, in accordance with the manufacturer's instructions. PCR was performed using KOD FX Neo (Toyobo). The PCR products were visualized by a FAS-IV gel imaging system (Nippon Genetics, Tokyo, Japan). Amplified products were confirmed by sequencing. Quantitative RT-PCR (RT-qPCR) was performed with TB Green Premix Ex Taq II (Takara, Otsu, Japan) and analyzed on a Thermal Cycler Dice Real-Time System II (Takara). Each cDNA sample was prepared in triplicate. TATA-binding protein (*TBP*) was used to normalize each

sample. The amount of each mRNA was evaluated by threshold cycle (Ct) values. The relative levels of each mRNA were evaluated by the values of $2^{[Ct\,(TBP)\,-\,Ct\,(each\,mRNA)]}$. Primer sets used in this study are listed in Table S3.

Assay for mini gene reporter fused *β-globin* FISH probe tag

U2OS cells on coverslips in a 12-well plate (20% confluence) were transfected with mini gene reporter fused *β-globin* FISH probe tag using Lipofectamine 2000 (Thermo Fisher Scientific), in accordance with the manufacturer's protocol, and cultured for 6 h. Then, each compound was added, and cells were further cultured for 24 h. Cells were fixed with 10% formaldehyde in PBS for 20 min and permeabilized with 0.1% Triton X-100 in PBS for 10 min. Cells were washed three times with PBS for 10 min to remove the detergent, once with 1× SSC containing 50% formamide for 5 min to exchange the buffer content, and hybridized with a FISH probe labeled at the 5' end with Alexa Fluor 546 (5'-cttcatccacgttcaccttgccccacagggcagtaacggcagacttctcctcaggagtcaggtgcaccat-3') overnight at 37°C in a humidified chamber. Cells were washed twice for 15 min at 42°C with 1× SSC/50% formamide and then washed for 5 min at 42°C with 2× SSC. Cells were prehybridized with ULTRAhyb-Oligo Hybridization Buffer for 1 h at 42°C in a humidified chamber, and then incubated overnight with 10 pmol Alexa Fluor 594-labeled oligo-dT$_{45}$ probe diluted with hybridization buffer. Cells were washed for 20 min each at 42°C with 2× SSC, 0.5× SSC, and 0.1× SSC. The nuclei were visualized with DAPI.

Mini gene splicing assay

The *β-globin* reporter was kindly provided by Michael Antoniou, Ph.D. (Antoniou et al., 1998) The *β-globin* gene was amplified using this reporter. The amplified product was digested with KpnI and HindIII and then cloned into the KpnI and HindIII sites of pcDNA5/FRT/TO vector (Invitrogen, Carlsbad, CA). The genomic fragment of the apigenin- and luteolin-target gene was amplified from human genome DNA by PCR using KOD FX Neo (Toyobo). The amplified product was digested with BamHI and XhoI, and then cloned into the BamHI and XhoI sites of pcDNA5/FRT/TO vector using the wild type as a template; mutations were introduced by two-step PCR, as illustrated in Figures 6B, 6C, and S6. These mini genes were confirmed by sequencing. U2OS cells (20% confluence) in a six-well plate were cultured for 24 h after inoculation, and then transfected with

mini gene using Lipofectamine 2000 (Thermo Fisher Scientific), in accordance with the manufacturer's protocol, and cultured for 6 h. Then, each compound was added, and cells were cultured for 24 h. cDNA was synthesized from total RNA using ReverTraAce (Toyobo) and random 9-mer primer, in accordance with the manufacturer's instructions. PCR was performed using pcDNA5/FRT/TO-specific primers. The amplified products were separated by 1.0% agarose gel or 8.0% polyacrylamide gel. Primer sets for this analysis are described in Table S3. The PCR products were visualized by a FAS-IV (Nippon Genetics). Band intensity was quantified by ImageJ, in accordance with the instructions.

MTT assay

Cell proliferation was assayed colorimetrically by 3-(4,5-di-methylthiazol-2-yl)-2,5-diphenyltetrazolium bromide, yellow tetrazole (MTT) (Sigma-Aldrich) assay. The cells were inoculated at 8×10^3 cells/mL in a 96-well plate and cultured for 24 h. The test samples were added to each cell culture well and incubated for 24, 48, or 72 h. After 5 μL of MTT reagent (5 mg/mL) had been added to each well, the cells were incubated for 4 h. The cell culture plate was centrifuged at 400×g for 5 min, after which the supernatant was removed. Then, the cells were solubilized with 10 mM NH_4Cl containing 10% SDS (pH 7.0). Cell proliferation was estimated by measuring the optical absorbance at 600 nm.

Preparation of RNA-seq library

U2OS cells were treated with DMSO, 75 μM apigenin, or 75 μM luteolin for 24 h and then harvested. Total RNA was extracted from them with Sepasol-RNA I Super G. RNA-seq library was prepared using Truseq Stranded mRNA Library Prep Kit (Illumina, San Diego, CA). RNA-seq was conducted with two biological replicates from each group using NextSeq High Output (Illumina).

RNA-seq and global splicing analysis

The obtained sequence reads were mapped to the human hg38 genome using STAR (version 2.5.2b) (Dobin et al., 2013). Alternative splicing analysis was performed by rMATS (version 3.2.5) (Shen et al., 2014). Nonsignificant splicing events were filtered out using the threshold of false discovery rate (FDR) < 0.05. Gene ontology (GO) analysis was performed using Database for

Annotation, Visualization and Integrated Discovery (DAVID: version 6.7) (Huang et al., 2009a, 2009b). Integrative Genomics Viewer (IGV: version 2.3) (http://software.broadinstitute.org/software/igv/home) was used for visualization of the mapping results. Events with an FDR less than 0.05 were defined as significant splicing events, and these events were analyzed by RT-PCR, RT-qPCR, and bioinformatic analysis. Splice site score was calculated using MaxEntScan (Yeo and Burge, 2004). BPS score was calculated using the SVM-BP program (Corvelo et al., 2010).

siRNA or plasmid transfection

Transfection of siRNA or pcDNA3.1-FLAG-SF3B1 (Item # 82576, obtained from Addgene, Watertown, MA) was performed using Lipofectamine 2000 (Thermo Fisher Scientific) according to the manufacturer's instructions. The knockdown was performed for 48 h in SF3B1 and for 40 h in TAP. EGFP siRNA was used as a control. The sequence of siRNAs used in this study is listed in Table S4.

SUPPLEMENTAL REFERENCES

Antoniou, M., Geraghty, F., Hurst, J., and Grosveld, F. (1998). Efficient 3'-end formation of human β-globin mRNA in vivo requires sequences within the last intron but occurs independently of the splicing reaction. Nucleic Acids Res. *26*, 721–729.

Corvelo, A., Hallegger, M., Smith, C.W.J., and Eyras, E. (2010). Genome-Wide Association between Branch Point Properties and Alternative Splicing. PLoS Comput Biol *6*, e1001016.

Dobin, A., Davis, C.A., Schlesinger, F., Drenkow, J., Zaleski, C., Jha, S., Batut, P., Chaisson, M., and Gingeras, T.R. (2013). STAR: Ultrafast universal RNA-seq aligner. Bioinformatics *29*, 15–21.

Finci, L.I., Zhang, X., Huang, X., Zhou, Q., Tsai, J., Teng, T., Agrawal, A., Chan, B., Irwin, S., Karr, C., et al. (2018). The cryo-EM structure of the SF3b spliceosome complex bound to a splicing modulator reveals a pre-mRNA substrate competitive mechanism of action. Genes Dev. *32*, 309–320.

Huang, D.W., Sherman, B.T., and Lempicki, R.A. (2009a). Bioinformatics enrichment tools: paths toward the comprehensive functional analysis of large gene lists. Nucleic Acids Res. *37*, 1–13.

Huang, D.W., Sherman, B.T., and Lempicki, R.A. (2009b). Systematic and integrative analysis of large gene lists using DAVID bioinformatics resources. Nat. Protoc. *4*, 44–57.

Shen, S., Park, J.W., Lu, Z., Lin, L., Henry, M.D., Wu, Y.N., Zhou, Q., and Xing, Y. (2014). rMATS: Robust and flexible detection of differential alternative splicing from replicate RNA-Seq data. Proc. Natl. Acad. Sci. U. S. A. *111*, E5593–E5601.

Yamazaki, T., Fujiwara, N., Yukinaga, H., Ebisuya, M., Shiki, T., Kurihara, T., Kioka, N., Kambe, T., Nagao, M., Nishida, E., et al. (2010). The Closely Related RNA helicases, UAP56 and URH49, Preferentially Form Distinct mRNA Export Machineries and Coordinately Regulate Mitotic Progression. Mol. Biol. Cell *21*, 2953–2965.

Yeo, G., and Burge, C.B. (2004). Maximum Entropy Modeling of Short Sequence Motifs with Applications to RNA Splicing Signals. J. Comput. Biol. *11*, 377–394.